4

Role of FGF and other related molecules in scarred and scar-free wound healing process

INTRODUCTION

It has been well perceived that any quiescent tissue of a eukaryotic living organism almost spontaneously evokes a reparative response when challenged with an injury. Nonetheless, the healing outcome might differ based on the extent and the site of injury. In vast majority of cases, the outcome of tissue healing is limited to small scale tissue repair wherein formation of a scarred tissue at the site of injury is observed (Gurtner et al., 2012; Jackson et al., 2012). However, even though rarely, in few instances the tissue heals by a scar free mechanism and proceeds till the lost structure is re-grown healing. Known as scar-free wound healing, in the latter case the epithelial cells rapidly cover the wound surface which later acts as an organizer to orchestrate the events leading to the structural and functional re-establishment of the lost part (Fergusson and O'Kane, 2004; Gurtner et al., 2008; Godwin and Rosenthal, 2014).

The scarred wound healing is achieved through a multifaceted yet overlapping sequence of event namely haemostasis, inflammation, proliferation and remodelling at the site of injury. There are ample records to believe that these events are tightly regulated by several mediators that include, but not limited to, platelets (Sonnemann and Bement 2011), inflammatory cells (Grose et al., 2002) cytokines (Glitzer and Goebeler, 2001), growth factors and matrix metalloproteinases (Madala et al., 2010). A tissue when injured would immediately relay signals to the cells at the site of injury to form a provisional matrix over the wound to curtail blood loss. Immediately following haemostasis, the newly recruited platelet cells trigger a local surge of inflammation (Mutsaers et al., 1997). Once the inflammation subdues the proliferation phase begins wherein the wound is rebuilt with granulation tissue which is a collection of fibroblasts, inflammatory cells, and neovasculature wrapped in a matrix of collagen and extracellular matrix. In the subsequent maturation phase, the granulation tissue undergoes substantial remodelling with attended retraction of blood vessels to form an avascular structure called scar, a dense collagen tissue, that thoroughly covers the wound (Enoch and Harding 2003; Diegelmann and Evans, 2004; Sonnemann and Bement, 2011). Not surprisingly, even the scar-free wound healing begins with a haemostasis phase, however, after an acute hike early

on, the inflammatory response is suddenly truncated, which is where the scar-free healing swerves away from that of the scarred one.

This abrupt drop in the inflammation marks the beginning of proliferation that allows the epidermal cells to rapidly divide and migrate as a layer to cover the wound surface which eventually stratifies to form multi-layered apical epithelial cap (AEC). The AEC, like an embryonic organizer, sends regulatory signals to the underlying mesenchyme and the latter responds by recruiting a pool of blastemal cells which proliferate and later get re-specified to recreate the lost tissue (Carlson, 2007). The various phases of scarred and scar-free wound healing are depicted in Figure 4.1.

Lizards regenerate a large variety and amount of tissues in the tail (Alibardi 1993, 1994, 2009; Lozito et al., 2016), but little tissue regeneration takes place in the limb (Marcucci 1930; Barber 1944, Bellairs and Bryant 1968, 1985). The interest on lizard tissue regeneration derives from the fact that these reptiles have a histological architecture similar to that of mammals, and can be considered a unique model for studies on tissue regeneration (in the tail) versus regeneration failure (in the limb). The lizard model of tissue regeneration (or failure) appears to be much closer to mammals than amphibians' broad regenerative capabilities (Harty et al., 2003). Considering this unique condition, lizards should represent a very useful experimental model to analyse the factors that limit tissue regeneration in the other amniotes (birds and mammals). The first step to tackle the problem of successful (in the tail) and failure (in the limb) of tissue regeneration relies on the detailed knowledge of the cytological process occurring after tail and limb amputation. Numerous studies have described in detail the process of regeneration in the tail (Hughes and New 1959; Simpson 1965; Cox 1969; Bellairs and Bryant 1985). Studies on lizard's limb specially the microscopic analysis after the amputation of limb is very limited (Kudokotsev, 1960) and thus in order to understand the healing pattern in limb, a detailed study on its histology was envisaged.

Further, wound healing, being an incredibly complex biological process with intricate molecular interaction amongst various cells at the site of injury, is modulated by the timed expression of a myriad of regulatory factors. Important among these factors are the members of epidermal growth factor (EGF), transforming growth factor beta (TGF-β), fibroblast growth factor (FGF), interleukin (IL) and tumour necrosis factor-α families (Penn et al., 2012; Makanae et al., 2016). In addition, vascular endothelial growth factor (VEGF), granulocyte

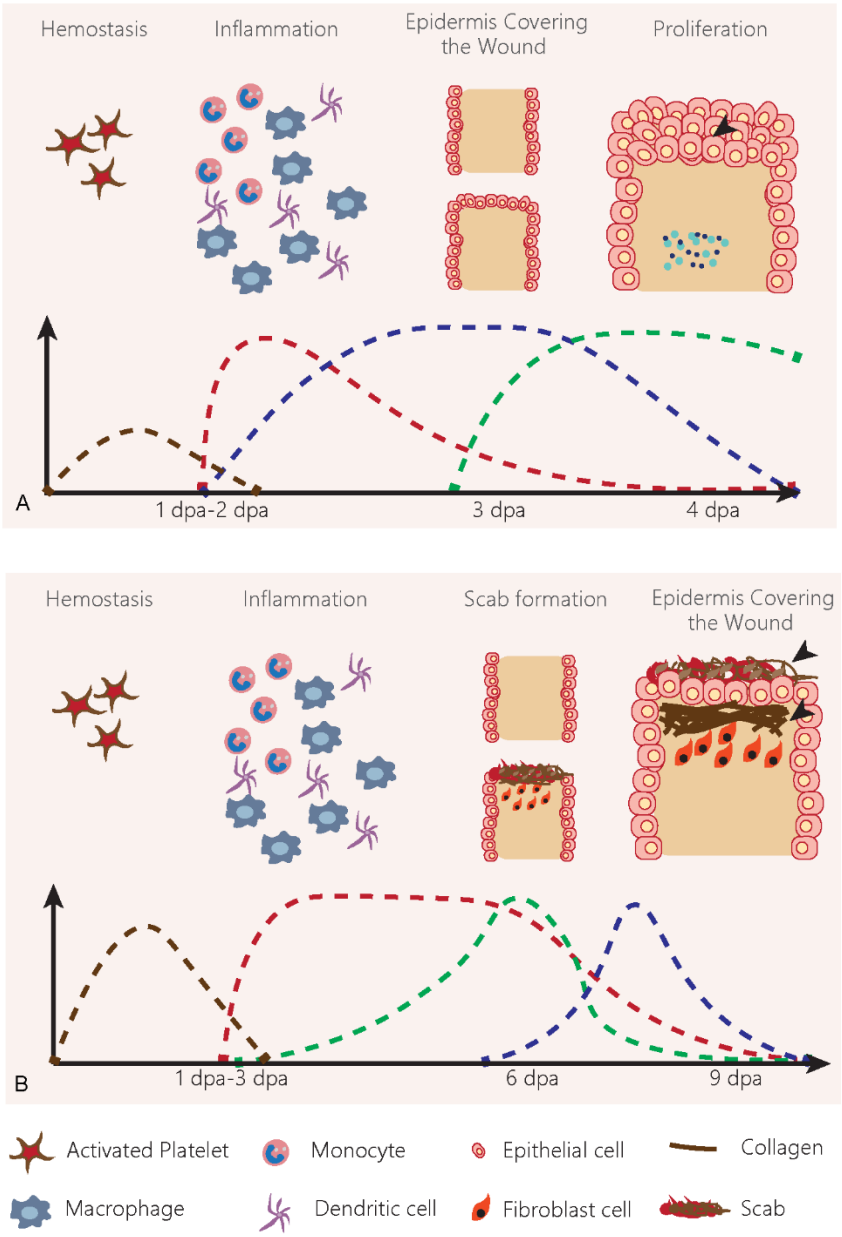

Figure 4.1: Phases in wound healing.

A) Depicts the scar-free wound healing where the epidermis covers the wound and then proliferates to form the Apical epithelial cap (AEC) as shown by the arrowhead. B) Shows the scarred wound healing where re-epithelialization starts along with fibroblast proliferation, deposition of collagen (shown by arrowheads) and ECM development to form the granulation tissue. Brown dotted line represents the hemostasis phase, red dotted line shows the inflammation phase, blue dotted line is for epidermis covering the wound and green dotted line depicts the proliferation of epidermis in scar-free wound healing while in scarred wound healing it represents proliferation of fibroblast cells and scab formation (adapted from Dieglemann and Evans, 2004; Murawala et al., 2018).

macrophage colony stimulating factor (GM-CSF), platelet-derived growth factor (PDGF), connective tissue growth factor (CTGF) are known to influence the process of wound healing (Barrientos et al., 2008; Matsumoto et al., 2014). Since the study foccuses on three processes, members of FGF and TGF-β were targeted as there are reports of these molecules being involved in proliferation, apoptosis and angiogenesis. Moreover, a temporal expression screening of these molecules is yet to be attempted in the appendages of lizard during the course of wound healing. Hence, it was thought pertinent to compare their expression pattern during the course of scarred as well as scar-free wound healing in the limb and the tail respectively of lizard *Hemidactylus flaviviridis*.

MATERIALS AND METHODS

Animal Maintenance:

Healthy adult northern house geckos of either sex having average snout to vent length of 10 cm were chosen for the study. They were acclimatized for a week and maintained all through the experiment in well ventilated wooden cages. The cages were housed in a room at a controlled temperature of 36±2 °C and 40-70 % relative humidity. The photoperiod was kept at 12 hours of light: dark cycle. Lizards were fed with cockroach nymphs daily and water was given *ad libitum*. Autotomy was induced in the tail by applying mild pressure with a foot ruler on the 3rd segment from the vent. The limb was amputated under hypothermia as a mode of inducing anaesthesia. Hypothermic shock was given by placing the animal on a pre-cooled tile and ice pack was applied to the limb to be amputated. With a sharp sterile surgical blade, the forelimb of the lizard was amputated. The experimental protocol (MSU-Z/IAEC/15-2017) was approved by the Institutional Animal Ethics Committee (IAEC) and all the experiments were performed as per the guidelines of Committee for the Purpose of Control and Supervision of Experiments on Animals (CPCSEA), India.

Experimental design

The tissue samples were harvested in a sterile condition at the selected time interval. Time points for tissue collection were decided based on the discrete events associated with wound healing in tail and in limb. These have been characterized for the tail through the course of various studies in our lab (Buch et al., 2017, 2018; Murawala et al., 2018). It has been observed that following autotomy of the tail, haemostasis is achieved rapidly and a scab is formed as early as 1 dpa. Subsequently, a thin layer of epithelium covers the wound surface on 2 dpa.

Thereafter, the epithelium continues to proliferate and stratifies into a multi-layered AEC that displaces the scab on 4 dpa. Hence the time points selected for tissue collection were 0 dpa (representing uncut resting stage), 1 dpa, 2 dpa, 3 dpa and 4 dpa.

On the other hand, wound healing in the amputated limb is achieved only on 9 dpa in the selected housing condition. Based on a continuous morphological observation on an amputated limb and as demonstrated in the previous studies by Alibardi, (2010) and Vitulo et al., (2017), the molecular events occurring therein were found to be different from that of tail. Haemostasis phase in case of amputated limb is longer compared to tail. Therefore, even on 3 dpa the cut end of limb shows only a scab with no development of epithelial layer beneath it. On 6 dpa, limb displays a thick blood clot and is in granulation phase. The complete formation of a proper scar is however, achieved on 9 dpa. Hence, the time points selected for limb were 0 dpa (representing uncut resting stage), 3 dpa, 6 dpa and 9 dpa. In this study we attempted to understand the molecular differences between the two modes of wound healing by designing the experiments composed of nine groups in total; five groups in case of tail and four groups for limb tissues. Each group consisted of six lizards for individual experiments. The tissues were processed as per the requirement described in the following sections.

Histology

Histological examination was performed for tail tissues at 0 dpa, 2 dpa and 4 dpa and at 0 dpa, 3 dpa and 9 dpa for limb tissues. The tissues were stored in 10 % neutral buffered formalin and decalcified by EDTA, followed by dehydration and embedding into paraffin blocks. Sections were cut at a thickness of 7 µm and stained with Harris' haematoxylin and eosin. The stained samples were observed under Leica DM2500 microscope and the representative digital images were grabbed using Leica EC3 camera. The microscopic measurements of various tissues in the tissue sections were done using LAS EZ software.

Immunohistochemistry

For immunolabelling, longitudinal cryosections (8-10 µm) were cut from freshly collected tissues, fixed in acetone at -20 ºC for 15-20 min and air dried for 15 min. Sections were then rehydrated with PBST (Phosphate Buffered Saline with 0.025 % Tween-20) followed by blocking with corresponding normal serum [Genei, Merck, USA; 10 % in PBS with 0.5 % Bovine serum albumin (PBS-BSA)] for 1 hr at room temperature (RT). Sections were then incubated with the antibody dilutions such as Anti-FGF2 IgG rabbit (Sigma Aldrich, USA, 0.5

µg/ml), Anti-VEGF-α IgG goat (Sigma Aldrich, USA, 0.1 µg/ml), Anti-cleaved Caspase 3 IgG goat (Sigma Aldrich USA, 0.1 µg/ml). For all primary antibodies, FITC-conjugated secondary antibodies (Sigma Aldrich USA, 0.1 µg/ml) were used and their expression was observed under a fluorescent microscope. The representative images were captured using a digital camera (Leica, EC3) mounted on the Leica DM2500 microscope.

BrdU labelling

Intraperitoneal injection of BrdU (Sigma Aldrich, USA) at a dose of 100 mg/kg body weight was given to the animals at 3 dpa and tail tissue was harvested at 4 dpa by inducing autotomy. In the case of the limb, BrdU was administered on 8 dpa and tissue was harvested for sectioning on 9 dpa. Tissues were embedded in cryo-embedding medium (Sakura Finetek, Japan) and fresh frozen sections (8-10 µm) were taken on 0.01 % poly-L-lysine coated slides. The sections were fixed in cold acetone (15-20 min at -20 ºC) and air dried for 15 mins followed by treatment with 2 N HCl for 30-60 min at 37 °C. Sections were blocked using the normal bovine serum albumin (10 % in PBS-BSA) for 1 hr at RT and incubated with 1:100 dilution of Mouse Anti-BrdU (Sigma Aldrich, USA) in PBS. Cold sections were later incubated with 1:50 dilution of Goat Anti-Mouse IgG-FITC (Genei, Merck, USA) in PBS for 2 hr at RT, washed, mounted with PBS:glycerol (1:1) and observed for the localisation using a fluorescence microscope (Leica DM2500 utilizing LAS EZ software).

Acridine orange and Ethidium Bromide staining

Cold sections (7 µm) were obtained using cryotome (Reichert-Jung Cryocut E, USA) to study the wound epithelium stage in tail at 4 dpa and scarring in limb at 9 dpa. The sections were washed with phosphate buffer of pH 7.4 (10 mM PO_4^{3-}, 0.137 M NaCl and 2.7 mM KCl) thrice. Following washing, AO/EtBr stain (100 µg/ml) was added for 10 sec and the sections were immediately washed with phosphate buffer. All the images were captured using a fluorescent microscope (Leica DM2500 utilizing LAS EZ software).

Western Blot

Tissues were harvested from all the nine groups and homogenized in lysis buffer (50 mM tris pH 7.5, 0.2 M NaCl, 10 mM $CaCl_2$ and 1 % triton-X 100) containing protease inhibitor. The samples were centrifuged at 12000 rpm for 10 min (4 ºC) and protein estimation was done using Bradford method (Bradford 1976). 40 µg of protein of each sample was loaded and resolved on a 12 % SDS-PAGE. These proteins were transferred onto PVDF membrane

through semi-dry transfer method by applying 100 mA for 25 min. The primary antibodies used to probe each protein of interest were Anti-cleaved Caspase 3 IgG goat (Sigma Aldrich USA, 0.1 µg/ml), Anti-Fibroblast growth factor 2 IgG rabbit (Sigma Aldrich USA, 0.1 µg/ml), Anti-VEGF-α IgG goat (Sigma Aldrich, USA, 0.1 µg/ml), Anti-GRB7 IgG mouse (DSHB USA, 0.5 µg/ml), Anti-PI3K IgG mouse (DSHB USA, 0.5 µg/ml), Anti-AKT IgG rabbit (Sigma Aldrich USA, 0.1 µg/ml), Anti-PCNA IgG rabbit (Sigma Aldrich USA, 0.1 µg/ml) and Anti- β-actin IgG mouse (Santa Cruz Biotechnology, USA, 0.01 µg/ml). The blot was developed by using the ALP, BCIP-NBT system (Sigma Aldrich, USA).

Quantitative Real-Time PCR

Total RNA was isolated from the limb and tail tissue homogenates using TRIzol reagent (Applied Biosystems, USA). One microgram of total RNA was reverse-transcribed to cDNA using a one-step cDNA Synthesis Kit (Applied Biosystems, USA). Primers were designed using PrimerBlast (NCBI), details of which are provided in Appendix I. Quantitative real-time PCR was performed on a LightCycler 96 (Roche Diagnostics, Switzerland) with the following program: 3 min at 95 ºC as initial denaturation step and 45 cycles with each cycle of 10 s at 95 ºC, 30 s at 60 ºC and 30 s at 72 ºC). Gel electrophoresis and melt curve analysis were used to confirm specific product formation. 18S rRNA was taken as endogenous control. The fold change was computed using method of Livak and Schmittgen (Livak and Schmittgen, 2011). In order to minimize variations among biological individuals, the tissue samples from six lizards were pooled and for each variable analysed in RT-PCR three technical replicates were performed to reduce the experimental error.

Statistical analysis

All the linear variables were organized as mean ± Standard Error of Mean. The measurements made in histology of limb was analysed using Unpaired t-test. Rest of the data were subjected to One-way ANOVA followed by Bonferroni Post-hoc test for multiple group comparison using GraphPad Prism software (GraphPad Software, Inc., San Diego, USA). A ‘p’ value of 0.05 or less was considered as being statistically significant.

RESULTS

Histology

Lizards, as a taxonomic group, are more closely related to mammals than are the urodeles. They are endowed with well-structured appendages to aid their terrestrial mode of life much akin to their mammalian counterparts. In the current study, the healing pattern in two different appendages, *viz.*, tail and limb, was assessed by investigating the histological changes of both, post-amputation and also during various stages of wound healing. Autotomy, when induced in the tail, leads to exposure of a variety of tissues like muscles and adipose along with the vertebral column (Figure 4.2 A). However, in the amputated limbs, in addition to the soft tissues mentioned earlier, humerus bone too was vividly seen in the histological section (Figure 4.5 A). Tail, being characterised as the fat storage organ of the lizard, exhibited thick layers of adipose tissue (Figure 4.2 A and 4.2 C), when compared to the limb (Figure 4.5 B and 4.5 C). As the bone can be seen protruding out from the limb (Figure 4.5 A), in tail the two lateral processes protrude conspicuously (Figure 4.2 B). In the tail after 2 dpa a proliferating epithelium was found to be covering the wound, as revealed in Figure 4.3 A with a mean thickness of 44.65 µm (Table 4.1; Figure 4.3 B). Later at 4 dpa (Figure 4.4 A) which is the WE stage, a thicker epidermis of 91.93 µm (Unpaired t-test; between 2 dpa and 4 dpa, $p \leq 0.001$) was observed (Table 4.1; Figure 4.4 B). However, on the lateral sides of tail the thickness of epithelium was 12.62 µm (Table 4.1; Figure 4.4 C). On the contrary when the amputated limb was monitored at 3 dpa, the epithelial layer was not visible on the wound surface (Figure 4.6 A), instead blood clot was seen to cover the open bone surface (Figure 4.6 B). At 9 dpa i.e. in the scarred limb tissue, a fully covered and healed structure was displayed, which differs significantly from previously described completely healed tail (4 dpa). Along with epithelium, a dense connective tissue was observed over the wound surface (Figure 4.7 A and 4.7 B). On the lateral side the mean thickness of connective tissue was 193.99µm (Table 4.2; Figure 4.7 C) while immediately over the wound it was 369.15 µm which was significantly high ($p \leq 0.001$) (Table 4.2; Figure 4.7 D). However, the newly formed epithelial layer was just 12 µm thick which is the normal thickness witnessed in the resting skin of limb and tail of lizard (Table 4.2; Figure 4.5 B).

Early proliferation of epithelium cells in tail contributes to scar-free wound healing

Members of FGF family have been known since long to induce and sustain cell proliferation at the site of amputation. Hence, their expression pattern was studied at mRNA level during

the wound healing phase of tail as well as limb in lizard (Figure 4.8 A and B). A steady increase in the mRNA levels of *fgf1, fgf2, fgf8,* and *fgf20* was observed in regenerating tail as healing progressed from 0 dpa to 4 dpa ($p \leq 0.001$) (Table 4.5; Figure 4.8 A). However, when the expression levels in all the stages were compared to that of resting stage i.e. 0 dpa, a sharp increase in fold change ($p \leq 0.001$) was noticed for *fgf10* on 3 dpa unlike the other fgfs screened (Table 4.5; Figure 4.8 A). In tandem with the increase in fgfs, *fgfr1* was also found elevated from 1 dpa to 4 dpa ($p \leq 0.001$) (Table 4.5; Figure 4.8 A). However, the limb healing stages which are 0, 3, 6 and 9 dpa showed a dissimilar trend to that observed in the tail. There was an increase in transcripts of *fgf1, fgf2, fgf8* and *fgf10* at 3 dpa but a sharp decline was observed in subsequent stages (Table 4.6; Figure 4.8 B). Moreover, the mRNA levels of *fgf20* and *fgfr1* were significantly downregulated ($p \leq 0.01$) at 3 dpa in limb as shown in Table 4.6 and Figure 4.8 B.

Furthermore, to find the actual trend of proliferation across the stages of wound healing, *pcna* at transcript level was studied and a steady increase was seen during tail wound healing stages with a 100-fold increase at 4 dpa, as compared to 0 dpa ($p \leq 0.001$) (Table 4.5; Figure 4.8 A). The healing limb also showed a progressive increase in *pcna* level but the fold change observed at 9 dpa was just 10-fold ($p \leq 0.001$) (Table 4.6; Figure 4.8 B). A concomitant western blot analysis of PCNA reaffirms the above findings as elevated levels of PCNA were found in tail healing stages and limb healing stages (Table 4.3 and 4.4; Figure 4.8 C and D), nonetheless, tail tissues showed a much a higher protein level than that in the limb (Table 4.3).

A confirmatory BrdU labelling also revealed the presence of proliferating epidermis and a pool of dividing cells underneath (Table 4.13; Figure 4.9 A). Quite contrary to the observations in the tail tissue, at wound epithelium stage (4 dpa) only faint signal of BrdU was observed in the scarred limb epithelium (9 dpa) indicating only basal levels of proliferation at a corresponding stage in the limb (Table 4.13; Figure 4.9 B).

Apoptosis is prominent in the scarred wound healing during the later phase

It is well perceived that immediately following injury the wound surface induces apoptosis to clear out the debris and in the subsequent phase of wound healing, regulated apoptosis facilitates a balanced proliferation and hence, transcript levels of *caspase3, bax, bad, cytC, p53, p23* and *bcl2* were quantified by real time PCR in the tissues collected from tail and limb during wound healing. On amputation of tail, within 1 dpa, a 2-fold increase in *caspase3* was observed

which remained persistent till 2 dpa (Table 4.7; Figure 4.10 A). Nevertheless, caspase3 returned to its basal levels at 3 and 4 dpa (Table 4.7; Figure 4.10 A). All the other apoptotic genes studied namely, *bax*, *bad*, *cytC*, *p53* and *p23* remained downregulated all through the healing stages of the tail (Table 4.7; Figure 4.10 A). However, in order to gain further insight into the regulation of apoptosis, expression pattern of anti-apoptotic gene *bcl2* was ascertained and it was observed that the transcript levels of *bcl2* remained subdued at the initial stages of healing tail, followed by an elevated expression at 3 and 4 dpa, understandably the observations being an exact contradiction to the observed levels of *caspase3* (Table 4.7; Figure 4.10 A). On the other hand, in the limb healing stages, except for *bad*, all the other genes remained downregulated at 3 dpa and 6 dpa (Table 4.8; Figure 4.10 B). At 9 dpa a sudden increase in the levels of *bax*, *cytC*, *p53* and *p21* was noted, while in the same time frame, *bcl2* showed an opposite trend in limb to that of the tail, as higher levels were found at 3 dpa and 6 dpa, which subsequently declined at 9 dpa (Table 4.8; Figure 4.10 B).

Western blot results of the cleaved Caspase 3 suggest the occurrence of persistent apoptosis in the tail from 0 dpa to 3 dpa and at the wound epithelium stage (4 dpa) this level drops perhaps to allows the proliferation to outcompete apoptosis (Table 4.3; Figure 4.10 C). However, the western blot image of the limb shows a steady increase in cleaved Caspase 3 bands from 0 dpa to 9 dpa (Table 4.4; Figure 4.10 D). Concomitantly, cleaved Caspase 3 was localized even in the tail at 4 dpa which did reveal a few cells undergoing apoptosis (Table 4.14; Figure 4.11 A and 4.11 B) however, in limb a large pool of cells was positively stained for cleaved Caspase 3 (Table 4.14; Figure 4.11 C and 4.11 D). These results coincide with the western blot and real time PCR outcomes.

Apart from the major genes involved in apoptosis, tgf-β levels were also screened as they have an important role in mediating apoptosis and wound healing. Both, *tgf-β1* and *tgf-β2* levels did not change significantly during the wound healing phase of the tail, but the scarring limb showed distinctly elevated expression of the same molecules, when compared to the resting tissue ($p \leq 0.001$) (Table 4.9; Figure 4.12 A). On the contrary, expression of *tgf-β3* showed an increasing trend in the tail from 1 to 4 dpa (Table 4.9; Figure 4.12 A) while its levels were found downregulated in limb from 3 dpa to 9 dpa (Table 4.10; Figure 4.12 B). Along with the ligands, tgf-β receptors were also screened and *tgf-βRI* was found to be upregulated at 9 dpa in limb (Table 4.10; Figure 4.12 B) and downregulated in the tail from 1 dpa to 4 dpa respectively (Table 4.9; Figure 4.12 A). *tgf-βRII* had a 2-fold increase in the tail from 1 dpa to 4 dpa ($p \leq$

0.05) (Table 4.9; Figure 4.12 A) but in limb no significant change was observed (Table 4.10; Figure 4.12 B).

In order to further validate these results, acridine orange and ethidium bromide staining was performed on fresh frozen sections of 0 dpa and 4 dpa tail tissue along with 0 dpa and 9 dpa tissues of the healing limb. Both, the tail and limb tissues at 0 dpa revealed live cells emitting green signal (Figure 4.13 A and B). By 4 dpa, in tail, a proliferating epidermis characterized by green fluorescence was predominantly observed along with few pro-apoptotic cells stained yellow (Figure 4.13 C and E). On the contrary the limb tissue on 9 dpa revealed heightened apoptosis marked by orange nuclear EtBr staining at the site of injury (Figure 4.13 D and F) which concurs with the gene expression pattern and western blot of cleaved Caspase 3.

Angiogenesis occurs early during the wound healing phase in tail but in the limb, it occurs late during granulation phase

Angiogenesis is regulated by molecules like vegf-α and kdr, which operate through PI3K/AKT pathway. Hence, initially at transcript level they were studied in all the stages of both, tail and limb wound healing. A progressive increase in *vegf-α* and *kdr* was noted from 1 to 4 dpa in tail following amputation ($p \leq 0.001$) (Table 4.11; Figure 4.14 A). However, in limb at 3 dpa, a downregulation of *vegf-α* and *kdr* was seen after which at 6 dpa stage a hike in transcript level was observed which again declined at 9 dpa (Table 4.12; Figure 4.14 B). However, the tail had a much higher transcript level of *vegf-α* at wound epithelium stage (4 dpa) than the limb at scarring stage (9 dpa).

A careful analysis of the western blot images of FGF2, PI3K, AKT and VEGFα showed an increasing trend in their protein level from 1 to 4 dpa in the tail (Table 4.3; Figure 4.15 A). In the limb similar to the status of transcript, the protein levels of VEGFα also showed decline at 3 dpa, however, contradictory to transcripts the protein level was found elevated even on 6 dpa and remained high till 9 dpa (Table 4.4; Figure 4.15 B). However, no significant change was observed in FGF2 levels in limb throughout the healing process (Table 4.4; Figure 4.15 B).

FGF2 and VEGF-α, being the major molecules required in the process of angiogenesis, were localized in the tail on 4 dpa and in the limb on 9 dpa. It was revealed that FGF2 and VEGF-α were profusely expressed in the AEC and the underlying tissue in tail at 4 dpa (Table 4.15 and 4.16; Figure 4.16 A and C), while only weak signals were obtained from the 9 dpa limb (Table 4.15 and 4.16; Figure 4.16 B and D).

Table 4.1: Thickness of epithelium (in µm) during different stages of wound healing in tail.

Tissue layers analysed	**Thickness in µm**
Lateral Epithelium (Normal resting stage)	12.52 ± 0.91
Epithelium Covering Wound at 2 dpa	44.65 ± 1.28***
Epithelium Covering Wound at 4 dpa	91.93 ± 3.89$^{***,\#\#\#}$

Values are expressed as mean ± SEM. Thickness of epithelium at 2 and 4 dpa was compared with the thickness lateral epithelium using One-way ANOVA followed by Bonferroni's Multiple Comparison Test, represented by asterisk. *** represents $p \leq 0.001$. Wound epithelium thicknesses of 2 dpa and 4 dpa were also compared with each other using the same test denoted by hash. $^{\#\#\#}$ represents $p \leq 0.001$, n=6 for all the groups.

Table 4.2: Thickness of epithelium and connective tissue (in µm) during different stages of wound healing in limb.

Tissue layers analysed	**Thickness in µm**
Lateral Connective tissue (Normal resting stage)	107.5 ± 4.51
Connective tissue at Wound site at 9 dpa	369.15 ± 21.79***
Lateral Epithelium (Normal resting stage)	17.75 ± 3.87
Epithelium Covering Wound at 9 dpa	12.78 ± 0.71

Values are expressed as mean ± SEM. Thickness of connective tissue at wound site was compared with that of the lateral side using Unpaired t-test denoted by asterisk. *** represents $p \leq 0.001$, n=6. The epithelium thicknesses of 9 dpa and lateral side were compared using Unpaired t-test which was found to be non-significant.

Table 4.3: Band intensities of the western blots obtained for the tail wound healing time points.

	Protein Band intensities (Mean ± SEM)				
PROTEIN	0 dpa	1 dpa	2 dpa	3 dpa	4 dpa
PCNA	8.25 ± 0.56	10 ± 0.33	15.04 ± 1.91	27.4 ± 3.27**	68.34 ±4.93***
Cl. Caspase 3	5.85 ± 0.85***	26.45 ± 2.83*	13.84 ± 1.56	9.45 ± 0.96	5.74 ± 0.52
PI3K	6 ± 0.079	6.5 ± 0.87	6.7 ± 0.9	19.87 ± 3.7*	25.56 ± 4.34**
VEGF-α	8.27 ± 0.089	14.5 ± 1.23	15.45 ± 1.45	29.41 ± 2.87***	39.1 ± 3.95***
FGF2	5.98 ± 0.035	9.32 ± 0.34	29.56 ± 3.98**	49.4 ± 5.76***	58.23 ± 0.49***
AKT	4.92 ± 0.7	6.89 ± 0.56	20.65 ± 3.9*	28.76 ± 4.87**	36.76 ± 2.87***

Values are expressed as Mean ± SEM, * p≤ 0.05, ** p≤ 0.01 and *** p≤ 0.001 (n=6).

Table 4.4: Band intensities of the western blots obtained for the limb wound healing time points.

	Protein Band intensities (Mean ± SEM)			
PROTEIN	0 dpa	3 dpa	6 dpa	9 dpa
PCNA	5.89 ± 0.35	6.54 ± 0.26	9.52 ± 1.51	16.71 ± 3.85*
Cl. caspase 3	3.85 ± 0.63	10.85 ± 1.56	12.83 ± 0.96*	35.85 ± 2.96***
PI3K	10.45 ± 0.76	6 ± 0.079***	2.9 ± 0.08***	1.5 ± 0.043***
VEGF-α	11.78 ± 0.98	2.6 ± 0.098*	2.5 ± 0.045*	19.49 ± 3.56
FGF2	5.89 ± 0.23	9.57 ± 0.81	15.82 ± 0.91***	18.34 ± 1.87***
AKT	4.21 ± 0.34	3.9 ± 0.08	10.54 ± 0.24**	16.83 ± 1.53***

Values are expressed as Mean ± SEM, * p≤ 0.05, ** p≤ 0.01 and *** p≤ 0.001 (n=6).

Table 4.5: Relative gene expression data for genes involved in proliferation during wound healing stages of lizards' tail

	Fold change (Mean ± SEM)			
Gene Name	**1 dpa**	**2 dpa**	**3 dpa**	**4 dpa**
fgf1	8.68 ± 0.54**	9.43 ± 0.745**	10.55 ± 0.98***	14.12 ± 1.11***
fgf2	2.87 ± 0.19*	3.75 ± 0.12*	3.82 ± 0.0987*	4.74 ± 0.21*
fgf8	3.79 ± 0.214*	4.32 ± 0.25*	4.56 ± 0.14*	7 ± 0.47**
fgf10	3.65 ± 0.11*	5.65 ± 0.33**	5.13 ± 0.68**	42 ± 1.101***
fgf20	1.21 ± 0.08	2.1 ± 0.098*	3.53 ± 0.101*	3.33 ± 0.13*
fgfr1	3.76 ± 0.147*	4.45 ± 0.18*	4.51 ± 0.25*	6.63 ± 0.47**
pcna	10.23 ± 0.78***	35.98 ± 2.1***	49.91 ± 3.12***	120 ± 9.8***

Values are expressed as Mean ± SEM, * p≤ 0.05, ** p≤ 0.01 and *** p≤ 0.001 (n=6).

Table 4.6: Relative gene expression data for genes involved in proliferation during wound healing stages of lizards' limb

	Fold change (Mean ± SEM)		
Gene Name	**3 dpa**	**6 dpa**	**9 dpa**
fgf1	2.54 ± 0.0085*	0.54 ± 0.04	0.41 ± 0.023*
fgf2	3.12 ± 0.0012*	0.01 ± 0.00078***	0.13 ± 0.01**
fgf8	3.87 ± 0.0032*	0.03 ± 0.0014***	1.1 ± 0.0968
fgf10	2.67 ± 0.0011*	0.01 ± 0.0009***	0.01 ± 0.00085***
fgf20	0.13 ± 0.0098**	0.14 ± 0.00098**	0.13 ± 0.0096**
fgfr1	0.13 ± 0.0087**	0.01 ± 0.00085***	0.02 ± 0.0014***
pcna	2.19 ± 0.101*	2.48 ± 0.13*	10.23 ± 1***

Values are expressed as Mean ± SEM, * p≤ 0.05, ** p≤ 0.01 and *** p≤ 0.001 (n=6).

Table 4.7: Relative gene expression data for genes involved in apoptosis during wound healing stages of lizards' tail

	Fold change (Mean ± SEM)			
Gene Name	**1 dpa**	**2 dpa**	**3 dpa**	**4 dpa**
caspase3	2.34 ± 0.034*	2.09 ± 0.11*	1.4 ± 0.087	0.99 ± 0.054
bcl2	0.1 ± 0.005**	0.23 ± 0.012*	1.5 ± 0.101	3.28 ± 0.28*
bad	0.32 ± 0.03*	0.04 ± 0.0025***	0.04 ± 0.0024***	0.02 ± 0.0011***
p53	0.04 ± 0.004***	2.2 ± 0.0035*	0.04 ± 0.0035***	0.03 ± 0.0024***
p21	0.12 ± 0.03**	0.09 ± 0.0075***	0.02 ± 0.0012***	0.02 ± 0.0013***
bax	1.44 ± 0.04	1.38 ± 0.12	1.49 ± 0.12	1.43 ± 0.1
cytC	1.34 ± 0.01	1.29 ± 0.11	1.88 ± 0.11	1.21 ± 0.098

Values are expressed as Mean ± SEM, * p≤ 0.05, ** p≤ 0.01 and *** p≤ 0.001 (n=6).

Table 4.8: Relative gene expression data for genes involved in apoptosis during wound healing stages of lizards' limb

	Fold change (Mean ± SEM)		
Gene Name	**3 dpa**	**6 dpa**	**9 dpa**
caspase3	1.01 ± 0.085	3.56 ± 0.24*	4.69 ± 0.37*
bcl2	2.57 ± 0.12*	9.02 ± 0.74**	0.2 ± 0.012*
bad	5.5 ± 0.34**	216.02 ± 19.8***	10.78 ± 1.01***
p53	0.13 ± 0.0087**	0.01 ± 0.00086****	3.74 ± 0.24
p21	0.19 ± 0.0086**	0.1 ± 0.0087**	4.43 ± 0.31*
bax	0.07 ± 0.0054***	0.04 ± 0.0037***	0.94 ± 0.084
cytC	0.05 ± 0.0042***	0.00141 ± 0.000121***	3.65 ± 0.268*

Values are expressed as Mean ± SEM, * p≤ 0.05, ** p≤ 0.01 and *** p≤ 0.001 (n=6).

Table 4.9: Relative gene expression data for genes of TGF-β family during wound healing stages of lizards' tail

	Fold change (Mean ± SEM)			
Gene Name	**1 dpa**	**2 dpa**	**3 dpa**	**4 dpa**
tgfß1	1.23 ± 0.087	1.43 ± 0.0966	1.87 ± 0.11	1.91 ± 0.092
tgfß2	1.61 ± 0.065	1.81 ± 0.0852	1.85 ± 0.0987	1.77 ± 0.042
tgfß3	2.43 ± 0.0875*	5.1 ± 0.47**	5.23 ± 0.258**	6.87 ± 0.42**
tgfßRI	0.59 ± 0.0321	0.65 ± 0.052	0.49 ± 0.035*	0.42 ± 0.039*
tgfßRII	2.11 ± 0.0999*	1.99 ± 0.057	2 ± 0.13*	2.77 ± 0.12*

Values are expressed as Mean ± SEM, * p≤ 0.05 and ** p≤ 0.01 (n=6).

Table 4.10: Relative gene expression data for genes of TGF-β family during wound healing stages of lizards' limb

	Fold change (Mean ± SEM)		
Gene Name	**3 dpa**	**6 dpa**	**9 dpa**
tgfß1	1.24 ± 0.087	3.21 ± 0.14*	8.36 ± 0.58**
tgfß2	1.39 ± 0.098	2.12 ± 0.11*	6.68 ± 0.47**
tgfß3	0.01 ± 0.00052***	0.02 ± 0.0014***	0.01 ± 0.00057***
tgfßRI	1.89 ± 0.047	2 ± 0.098	2.3 ± 0.087*
tgfßRII	1.56 ± 0.068	2.02 ± 0.085*	1.8 ± 0.086

Values are expressed as Mean ± SEM, * p≤ 0.05, ** p≤ 0.01 and *** p≤ 0.001 (n=6).

Table 4.11: Relative gene expression data for genes involved in angiogenesis during wound healing stages of lizards' tail

	Fold change (Mean ± SEM)			
Gene Name	**1 dpa**	**2 dpa**	**3 dpa**	**4 dpa**
vegfα	1.82 ± 0.095	30.23 ± 2.4***	34.12 ± 2.14***	87.89 ± 6.45***
kdr	10.92 ± 0.12***	10.32 ± 0.17***	15.78 ± 1.14***	29.94 ± 1.89***

Values are expressed as Mean ± SEM, *** $p \leq 0.001$ (n=6).

Table 4.12: Relative gene expression data for genes involved in angiogenesis during wound healing stages of lizards' limb

	Fold change (Mean ± SEM)		
Gene Name	**3 dpa**	**6 dpa**	**9 dpa**
vegfα	0.14 ± 0.0085**	5.13 ± 0.76**	0.12 ± 0.0088**
kdr	0.13 ± 0.0078**	8.23 ± 1.1**	0.22 ± 0.014*

Values are expressed as Mean ± SEM, * $p \leq 0.05$ and ** $p \leq 0.01$ (n=6).

Table 4.13: Fluorescence intensity measured for BrdU positive cells

Tissue	**Intensity (AU)**
Tail (4 dpa)	12.545 ± 1.4
Limb (9 dpa)	2.42 ± 0.098***

Values are expressed as Mean ± SEM, *** $p \leq 0.001$ (n=6).

Table 4.14: Fluorescence intensity measured for cleaved Caspase 3 positive cells

Tissue	**Intensity (AU)**
Tail (4 dpa)	11.447 ± 1.56
Limb (9 dpa)	32.516 ± 3.78***

Values are expressed as Mean ± SEM, *** p≤ 0.001 (n=6). (Statistical test: Student's t-test)

Table 4.15: Fluorescence intensity measured for FGF2 positive cells

Tissue	**Intensity (AU)**
Tail (4 dpa)	14.107 ± 1.42
Limb (9 dpa)	2.497 ± 0.43***

Values are expressed as Mean ± SEM, *** p≤ 0.001 (n=6). (Statistical test: Student's t-test)

Table 4.16: Fluorescence intensity measured for VEGF-α positive cells

Tissue	Intensity (AU)
Tail (4 dpa)	14.864 ± 1.59
Limb (9 dpa)	1.545 ± 0.08***

Values are expressed as Mean ± SEM, *** p≤ 0.001 (n=6). (Statistical test: Student's t-test)

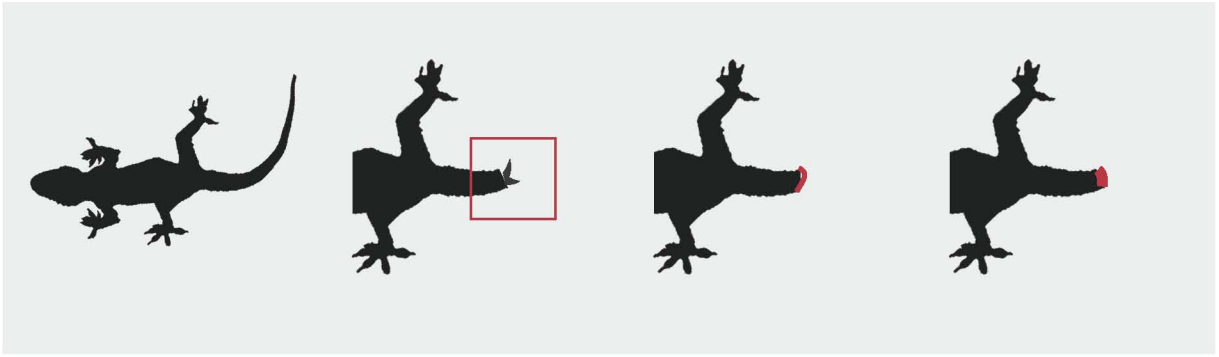

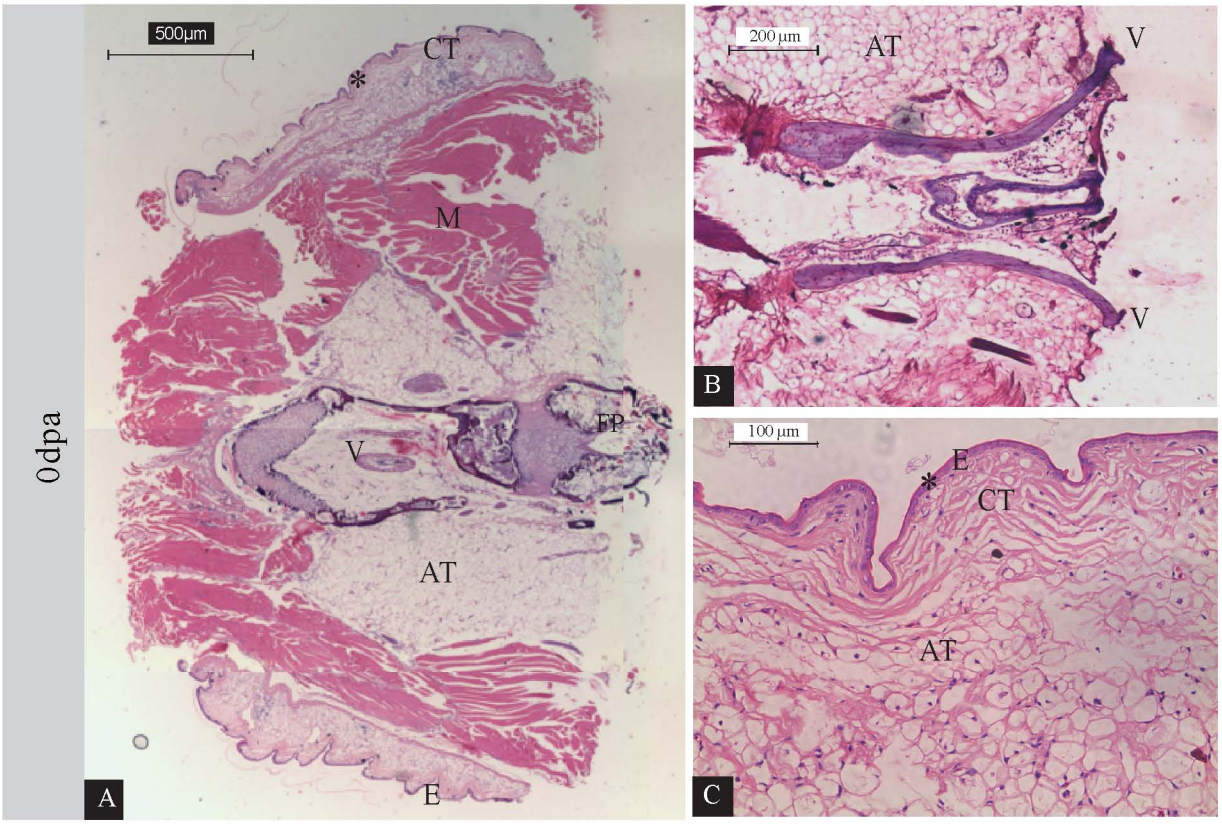

Figure 4.2: Histology of tail at 0 dpa

A) Longitudinal section of tail showing fracture plane (FP), muscles (M), adipose tissue (AT), epithelium (E) and connective tissue (CT) following tail autotomy; B) Magnified image of resting tail showing the vertebral column processes (V) projecting out; C) Magnified image showing arrangement of E, CT and AT. '*' represents the area magnified from image A. Magnification for A is 40X, B is 100X and C is 200X , n=6. The sections were stained with Haematoxylin and Eosin.

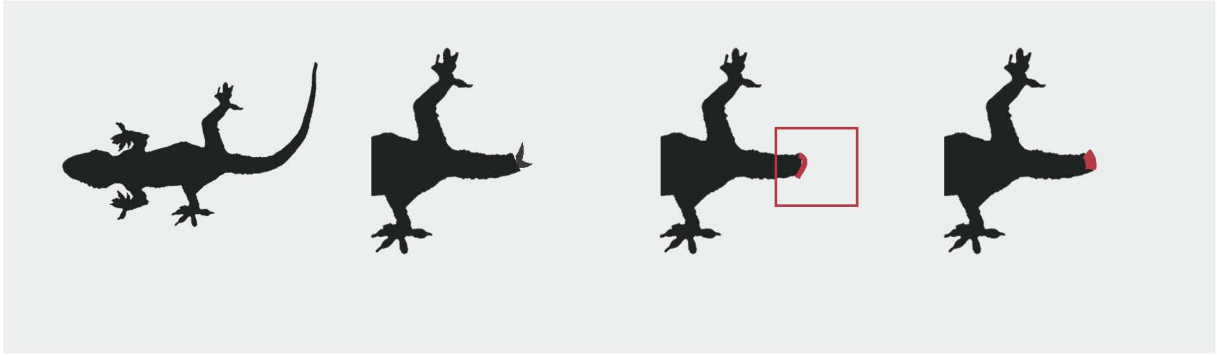

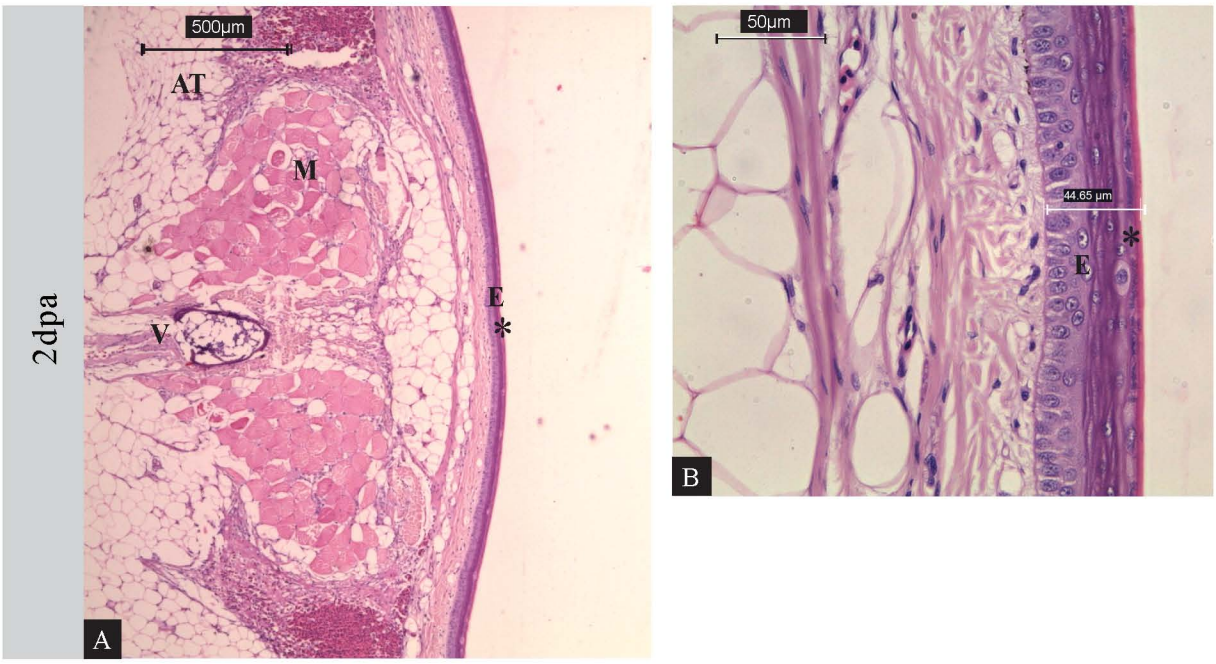

Figure 4.3: Histology of tail at 2 dpa

A) Epidermis covering the wound surface at 2dpa and B) The thickness of epithelium formed is 44.65 µm. Muscles (M), adipose tissue (AT), epithelium (E) and Vetebral column (V).'*' represents the area magnified from image A.
Magnification for A is 40X and B is 400X n=6. The sections were stained with Haematoxylin and Eosin.

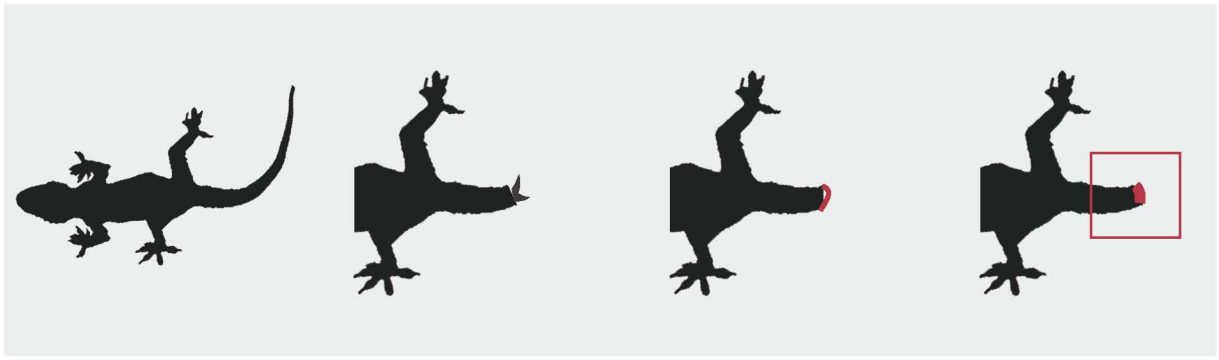

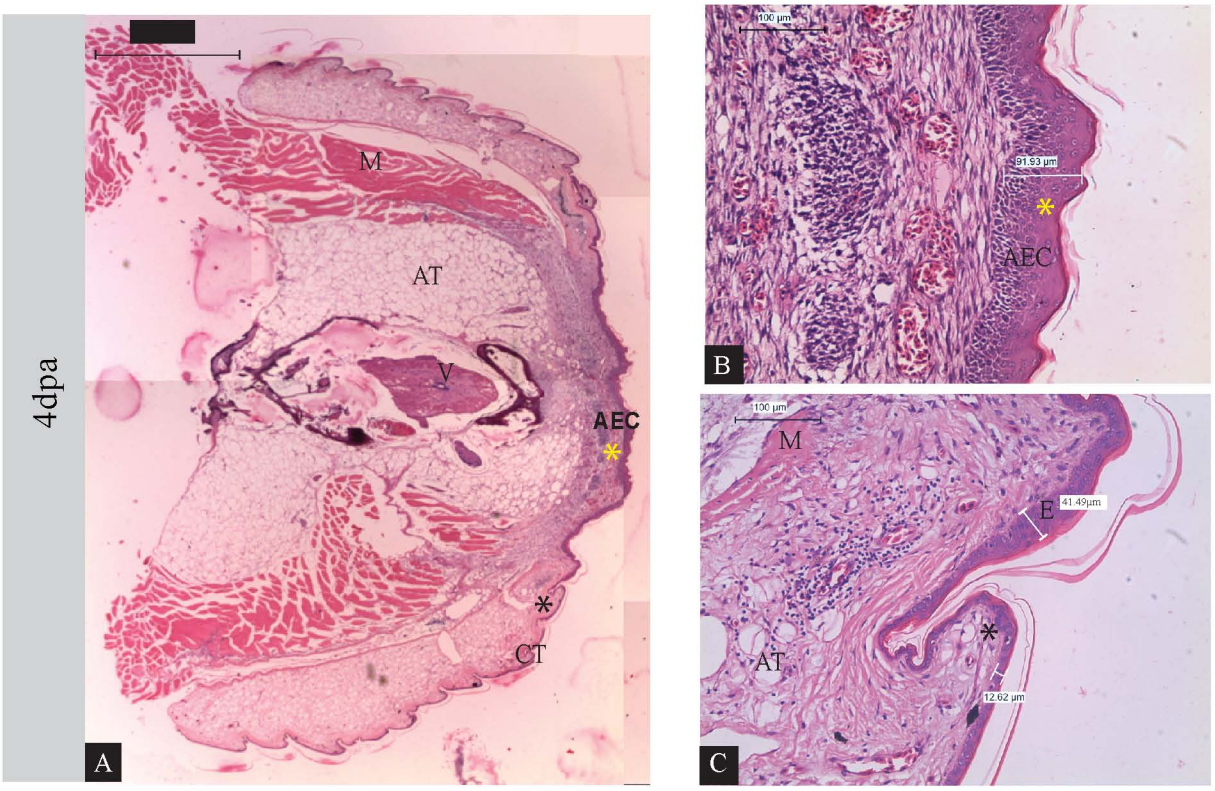

Figure 4.4: Histology of tail at 4 dpa

A) At 4 dpa, wound epithelium formation occurs that is depicted by proliferating epidermis also called as apical epithelial cap (AEC); (B) shows the magnified image of AEC by arrow which has a thickness of 91.93 µm; C) This section clearly shows that lateral epidermis maintains its thickness at 12.62 µm whereas the epidermis moving towards the AEC has a thickness of 41.49 µm. Muscles (M), adipose tissue (AT), epithelium (E) and Vetebral column (V)'*' represents the area that has been shown in the magnified image. All the sections are longitudinal in orientation and stained with hematoxylin eosin. Magnification for A is 40X,B and C is 200X, n=6.

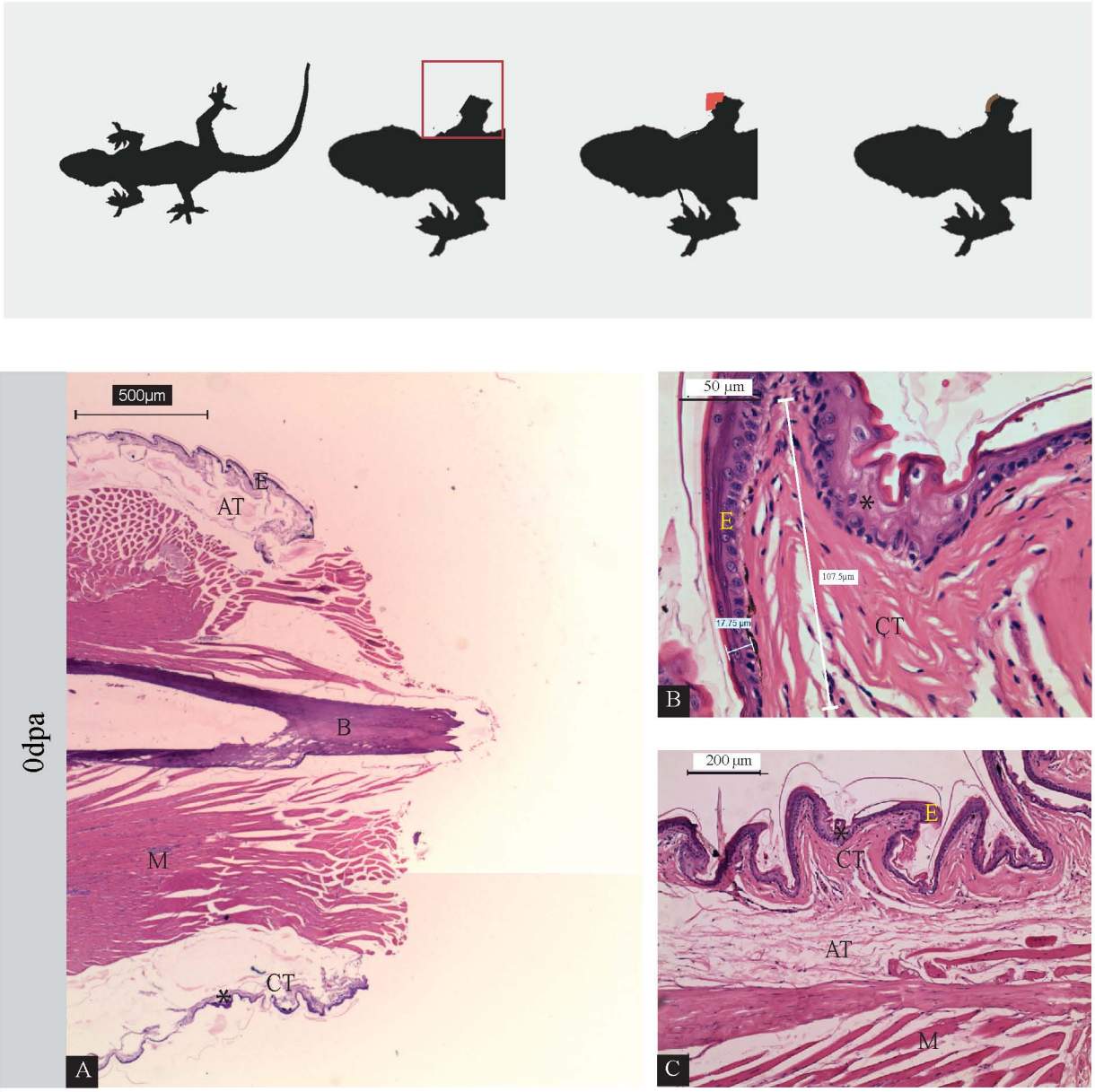

Figure 4.5: Histology of limb at 0 dpa

A) The limb, which on amputation shows exposed tissues like muscles (M), connective tissues (CT), humerus bone (B), epithelium (E) and adipose tissue (AT); B) Enlarged image showing connective tissue with a thickness of 107.5 µm and epithelium having same thickness as that of tail which is 17.75 µm; C) Arrangement of tissues can be observed which is similar to that of tail except AT being thicker in tail and CT being comparatively thicker in limb. '*' represents the area that has been shown in the magnified image. All the sections are longitudinal in orientation and stained with hematoxylin eosin. Magnification for A is 40X, C is 100X, B is 400X, n=6.

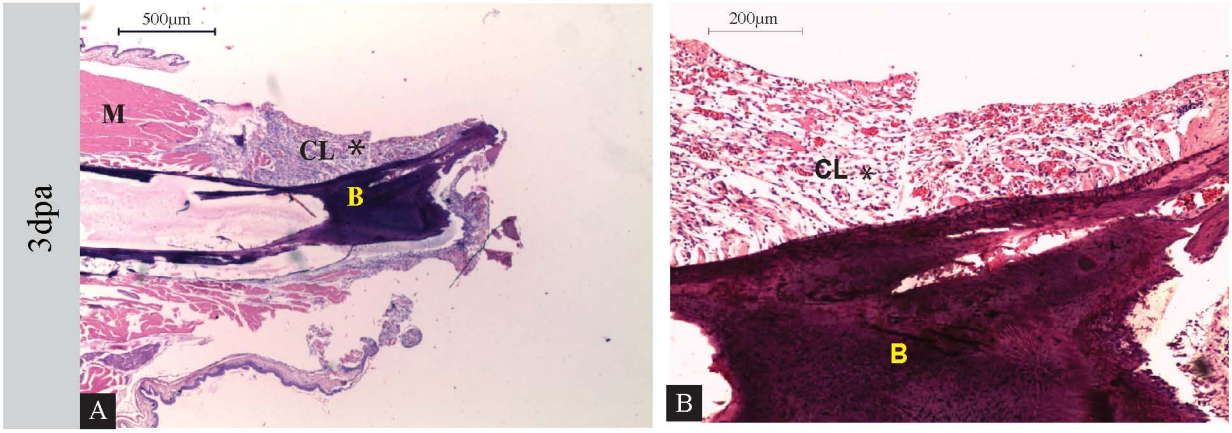

Figure 4.6: Histology of limb at 3 dpa

A) displays histology of limb at 3 dpa with no epithelium covering and B) represents persistent blood clot over the bone. muscles (M), connective tissues (CT), humerus bone (B), epithelium (E) and adipose tissue (AT). '*' represents the area that has been shown in the magnified image. All the sections are longitudinal in orientation and stained with hematoxylin eosin. Magnification for A is 40X, C is 100X, E is 400X, n=6.

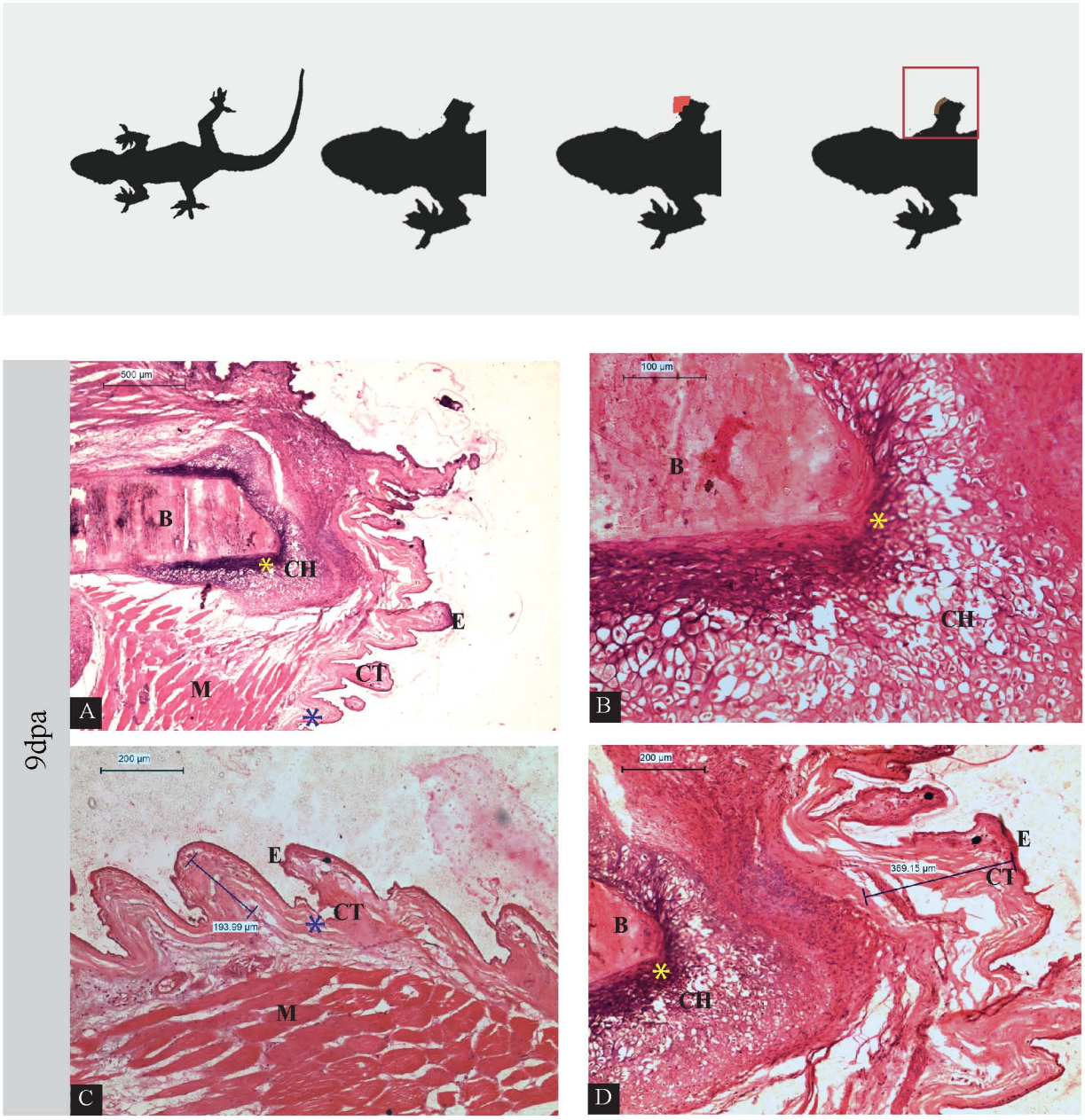

Figure 4.7: Histology of limb at 9 dpa

A) shows the healed limb wherein connective tissue (CT) can be observed covering the wound surface; B) depicts the chondrocytes which replace the clot over the humerus bone; C) shows lateral connective tissue with no difference in thickness from that of resting limb whereas in D) just at the wound site the thickness of connective tissue in 369.15 µm. '*' represents the area that has been shown in the magnified image. All the sections are longitudinal in orientation and stained with hematoxylin eosin. Magnification for A is 40X, C and D are 100X, B is 200X, n=6.

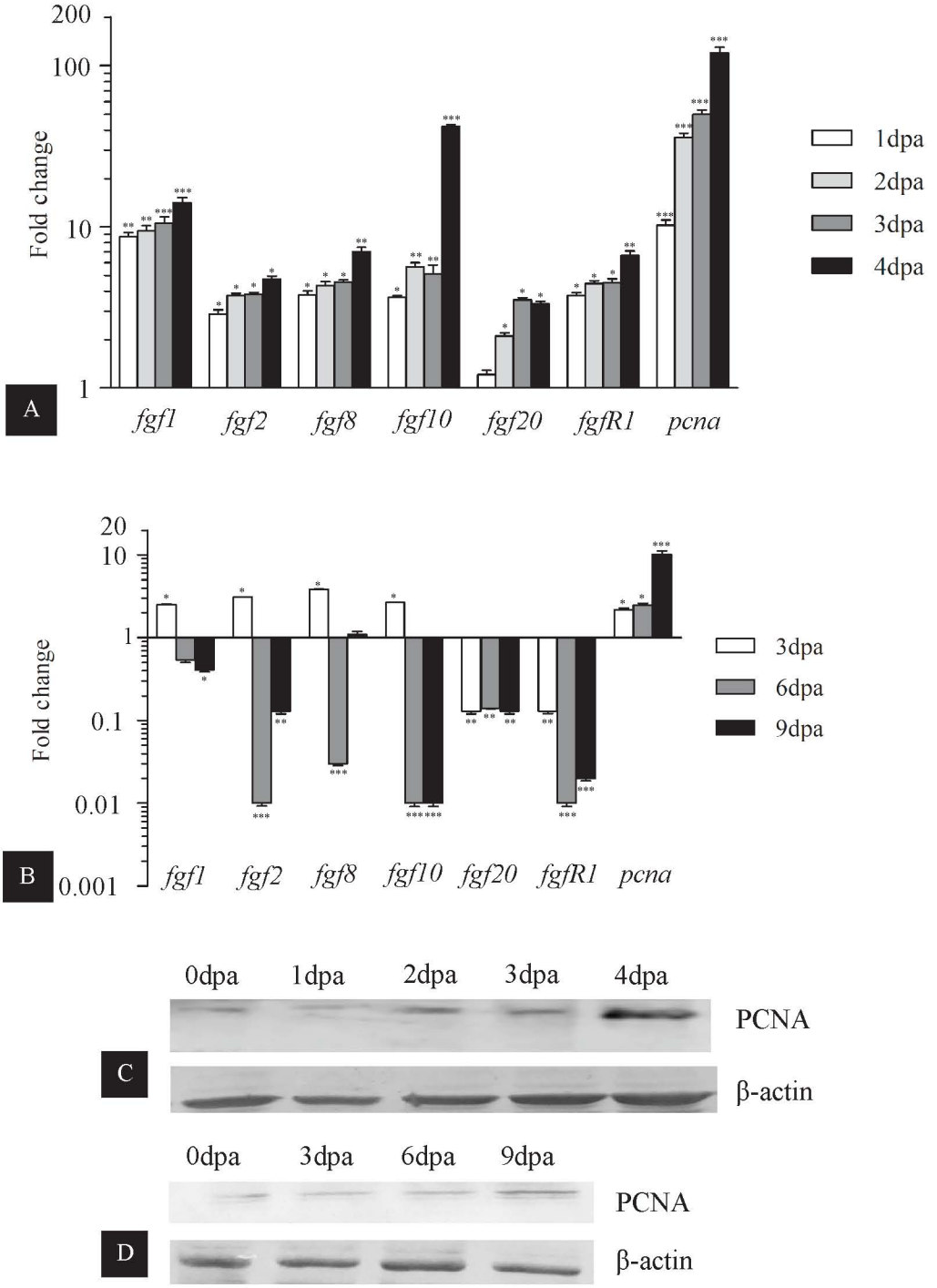

Figure 4.8: Gene expression and western blot of molecules involved in the process of cell proliferation during tail and limb wound healing

A) Relative transcript level expression of fgfs and pcna in tail wound healing. Fold change values for time points was normalized with that of the resting stage of tail. B) Relative transcript level expression of fgfs and pcna during limb wound healing. Fold change values for time points was normalized by those of the resting stage of limb. Error bars represent standard error of mean and asterisk represent p value where * represents $p \leq 0.05$, ** stands for $p \leq 0.01$ and *** depicts $p \leq 0.001$, (n=6); C) and D) depicts western blot of PCNA for tail and limb wound healing stages respectively

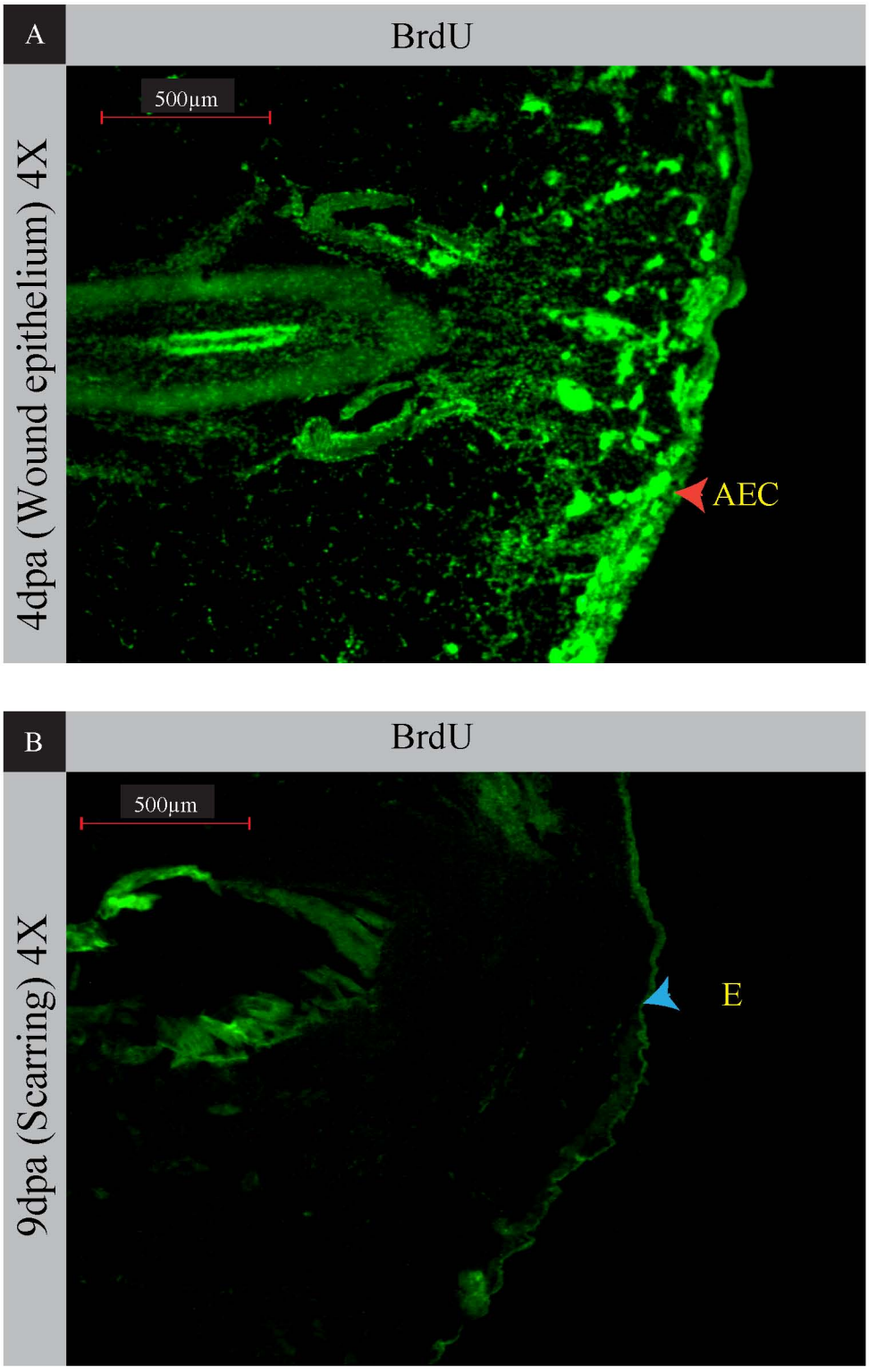

Figure 4.9: BrdU labelling for 4dpa and 9dpa in tail and limb respectively

A) and B) are the images for tail at 4dpa and limb at 9dpa showing BrdU incorporation wherein orange arrowhead shows the BrdU labelling in AEC and blue arrowhead represents the epithelium which is minimally representing BrdU in limb.

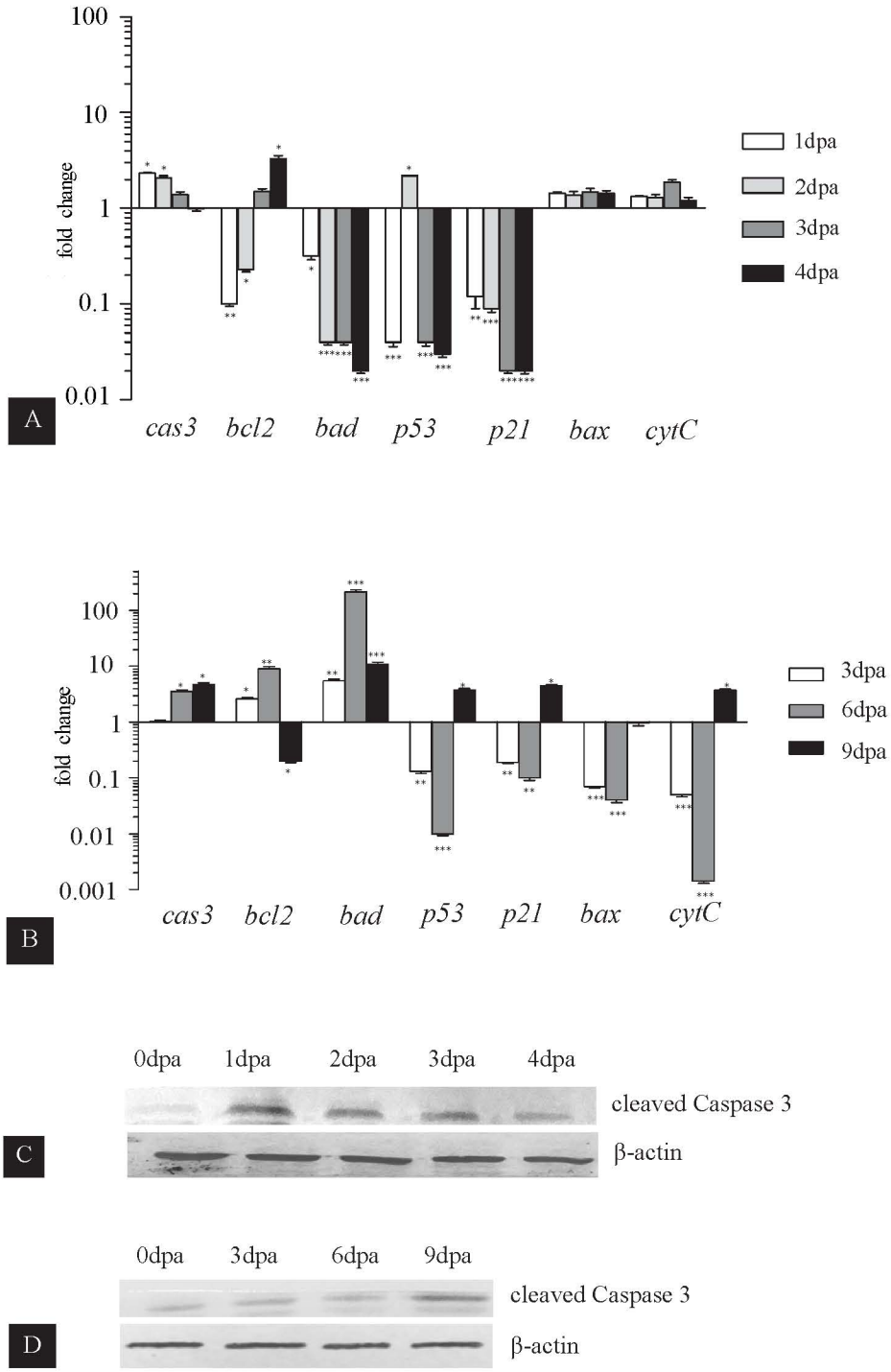

Figure 4.10: Gene expression and western blot of molecules involved in the process of apoptosis during tail and limb wound healing

A) Relative transcript level expression of apoptotic markers during wound healing in tail. Fold change values for time points was normalized with those of the resting stage of tail. B) Relative transcript level expression of apoptotic markers during wound healing in the limb. Fold change values for time points was normalized with those of the resting stage of limb. Error bars represent standard error of mean and asterisk indicates p value where * shows $p \leq 0.05$, ** depicts $p \leq 0.01$ and *** stands for $p \leq 0.001$. Figure C and D represent he western blot of cleaved caspase 3 in the wound healing stages of tail and limb respectively.

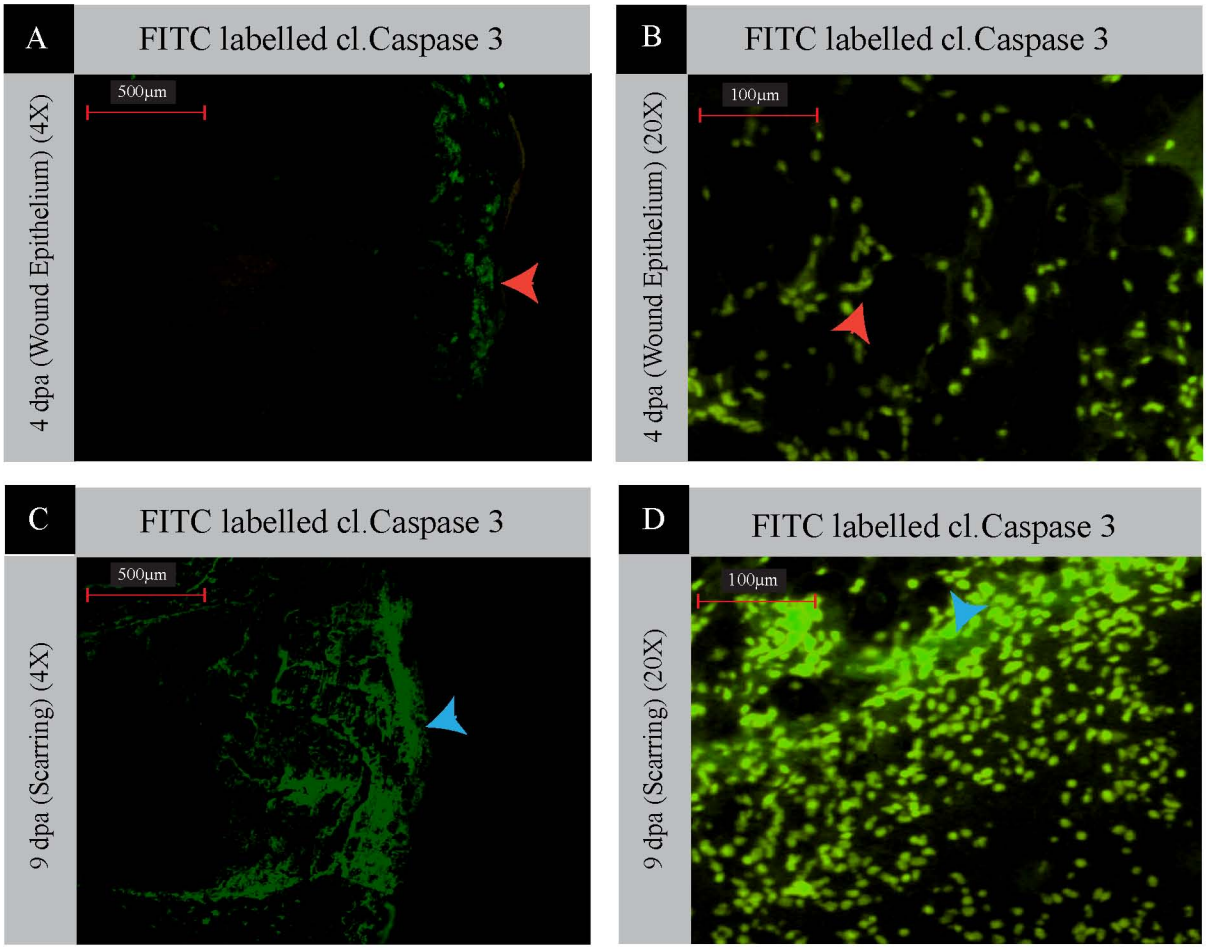

Figure 4.11: cleaved Caspase 3 localization

Figure A and B displays IHC for cleaved Caspase 3 in the tail at 4 dpa shown by orange arrowhead and Figure C and D represent the positive immuno staining for limb at 9 dpa depicted by blue arrowhead.

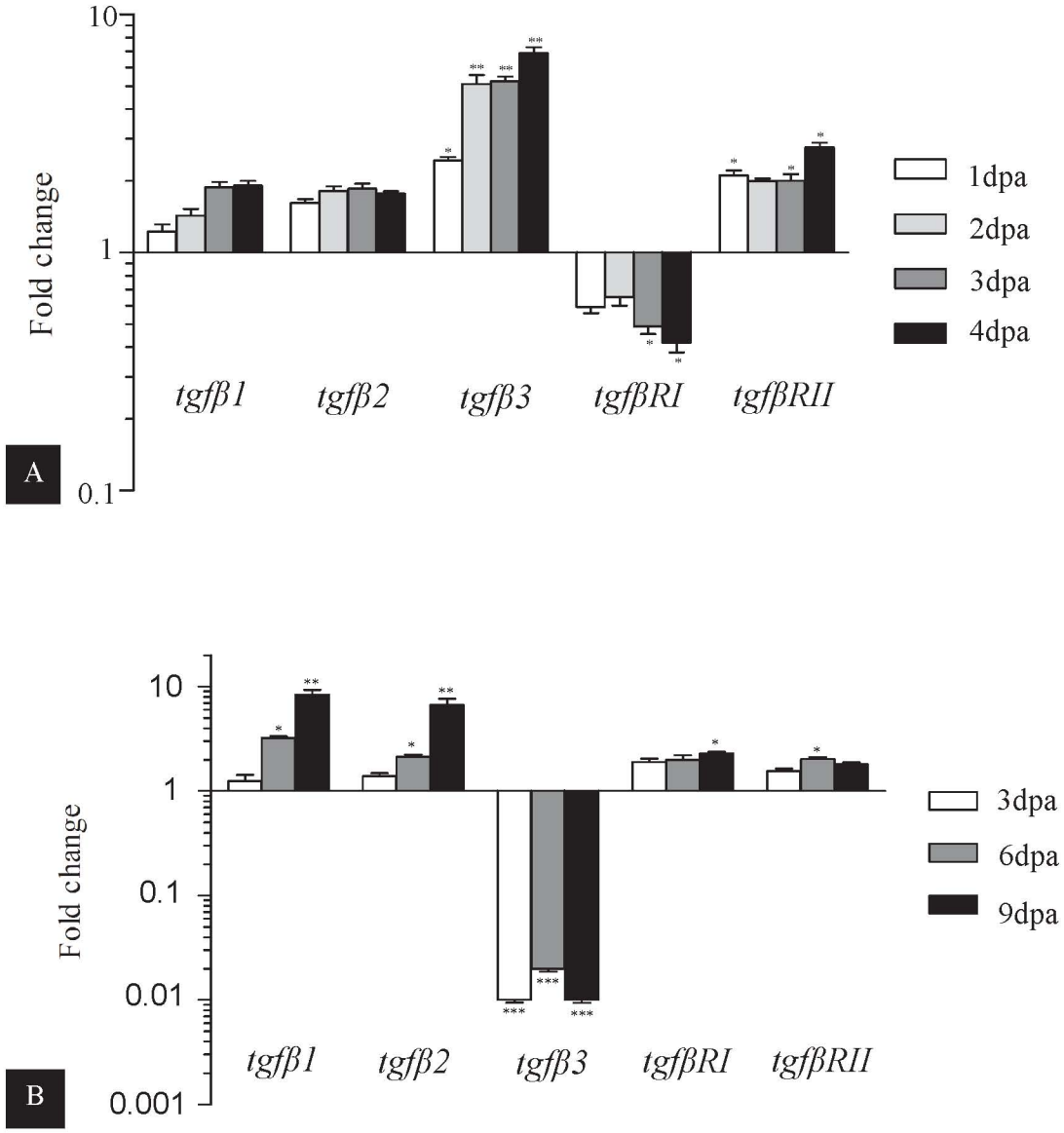

Figure 4.12: Gene expression of tgfβ family members

A) and B) denote fold change values of tgf-β in tail and limb wound healing stages where error bars exemplify standard error of mean and asterisk represent p value where * stands for $p \leq 0.05$, ** shows $p \leq 0.01$ and *** illustrates $p \leq 0.001$;(n=6)

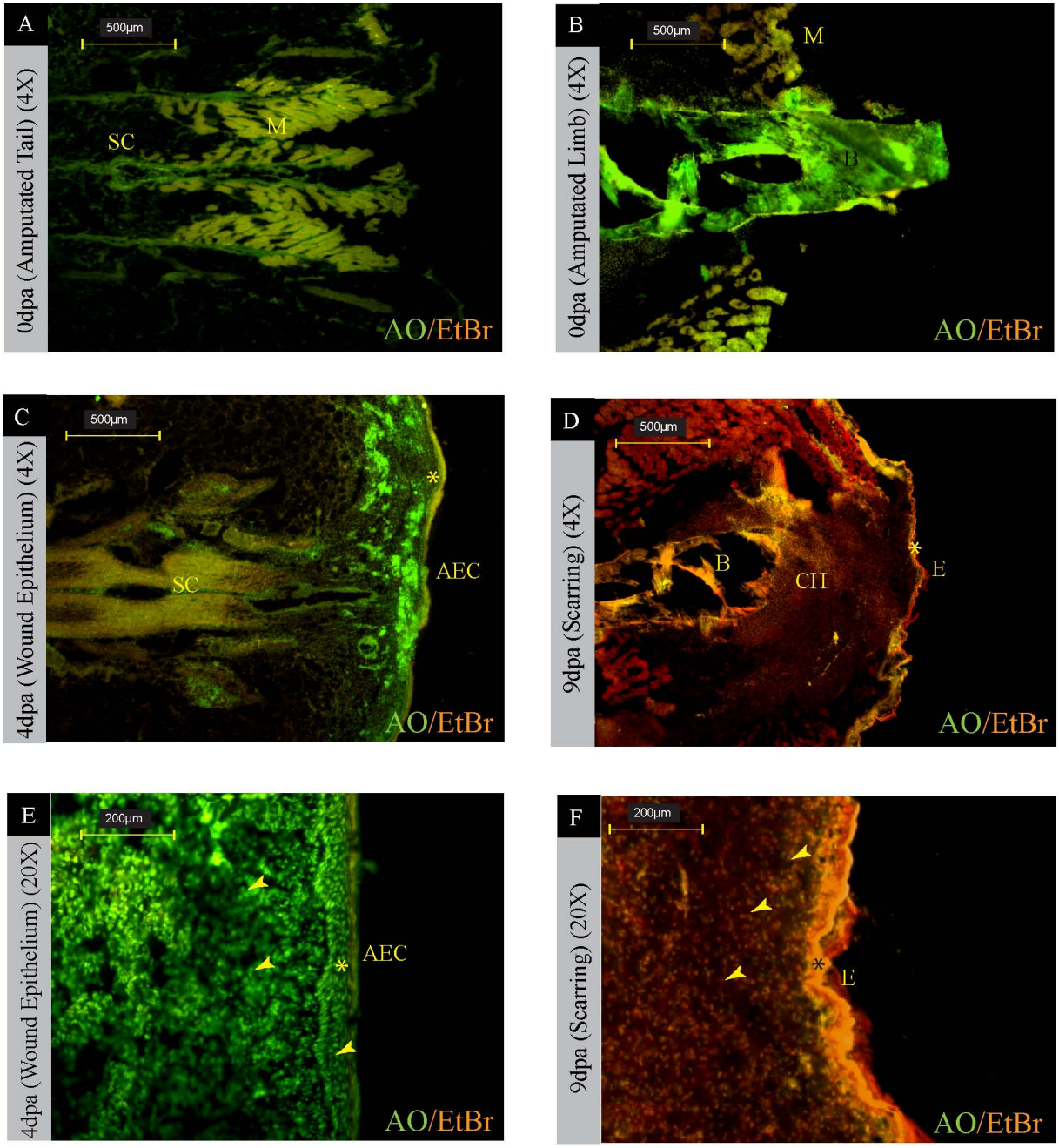

Figure 4.13: Acridine orange and ethidium bromide staining of tail and limb tissues

Figure A-F represent acridine orange and ethidium bromide staining wherein K and L are the tail and limb post amputation while M and N are the wound healing stages for tail and limb and their higher magnified images are O and P. The arrow heads in figure O denotes. the live cells which are visible due to green fluorescence whereas arrow head in figure P depicts the pro and apoptotic cells which are orange and red in color respectively. "*" represents the area which is depicted in the magnified image. (AEC: apical epithelial cap, B: bone, CH: chondrocytes E: epithelium, M: Muscle, SC: spinal cord,).

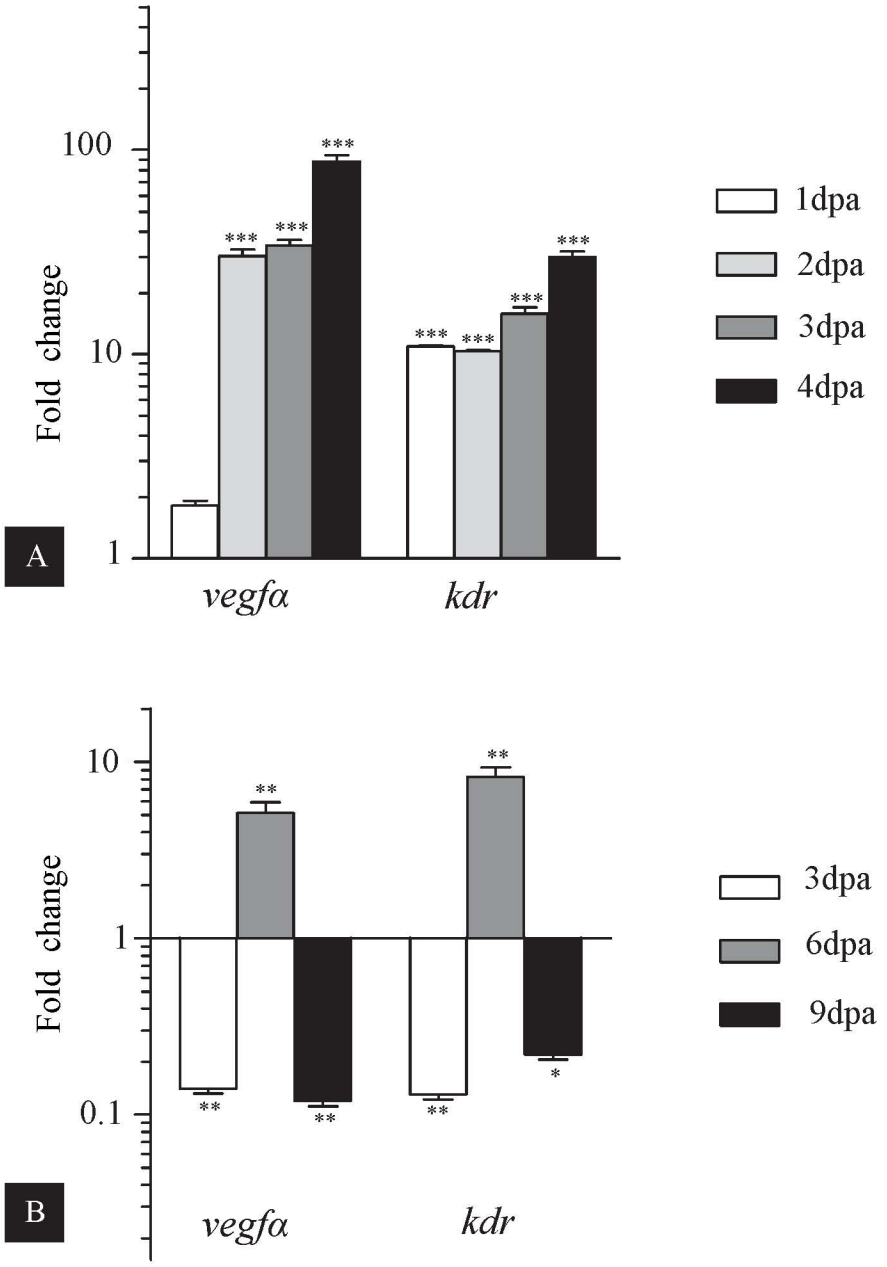

Figure 4.14: Gene expression for molecules involved in the process of angiogenesis

A) Relative transcript level expression of vegf-α and kdr in tail wound healing. Fold change values for time points was normalized with those of the resting stage of tail. B) Relative transcript level expression of vegf-α and kdr in limb wound healing. Fold change values for time points was normalized with the values of the resting stage of limb. Error bars represent standard error of mean and asterisk depicts p value where * highlights $p \leq 0.05$, ** marks $p \leq 0.01$ and *** stands for $p \leq 0.001$;(n=6)

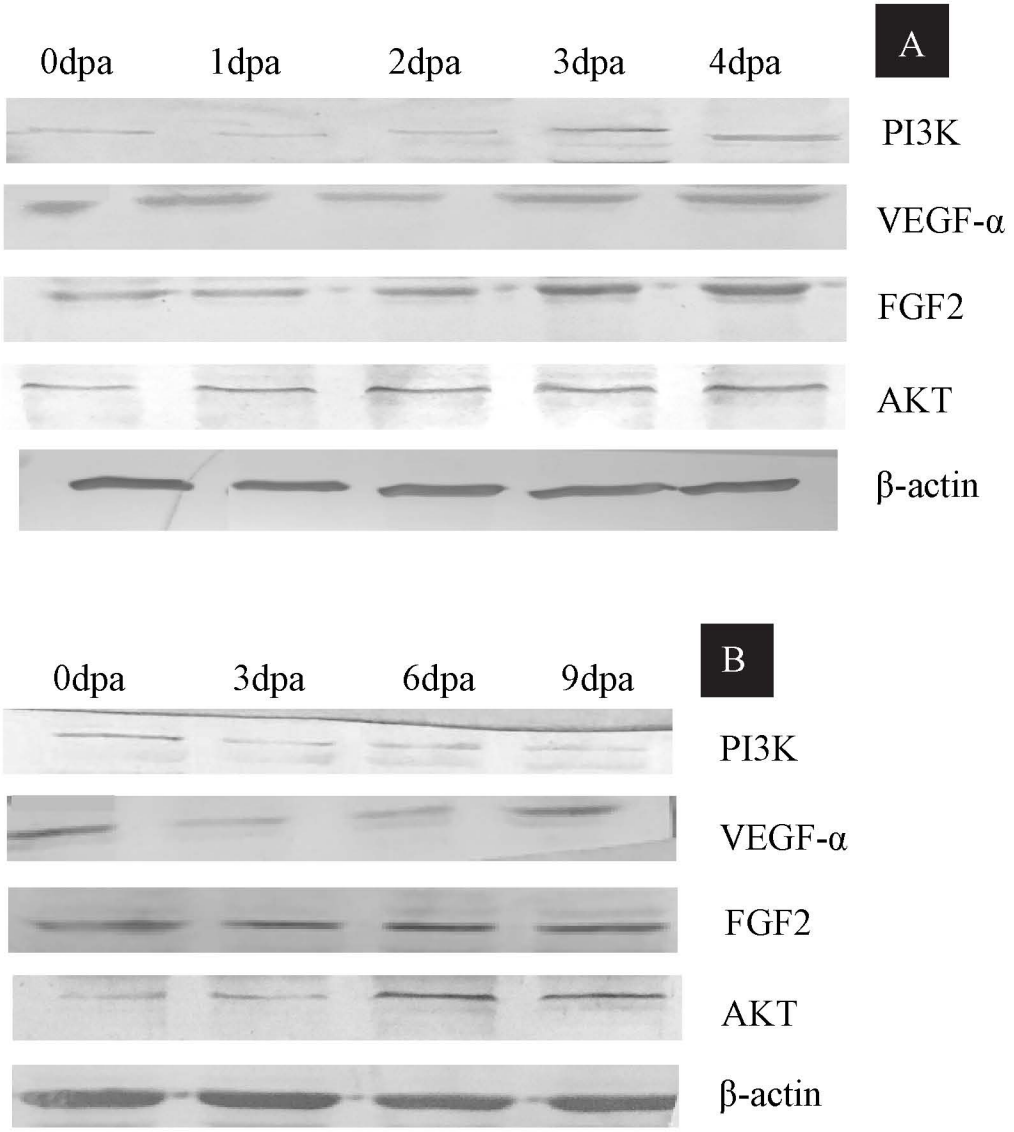

Figure 4.15: Western blot for molecules involved in the process of angiogenesis

A) and B) Western blot of VEGF-α, FGF2, PI3K and Akt for wound healing stages of tail and limb respectively, where β-actin was taken as the loading control

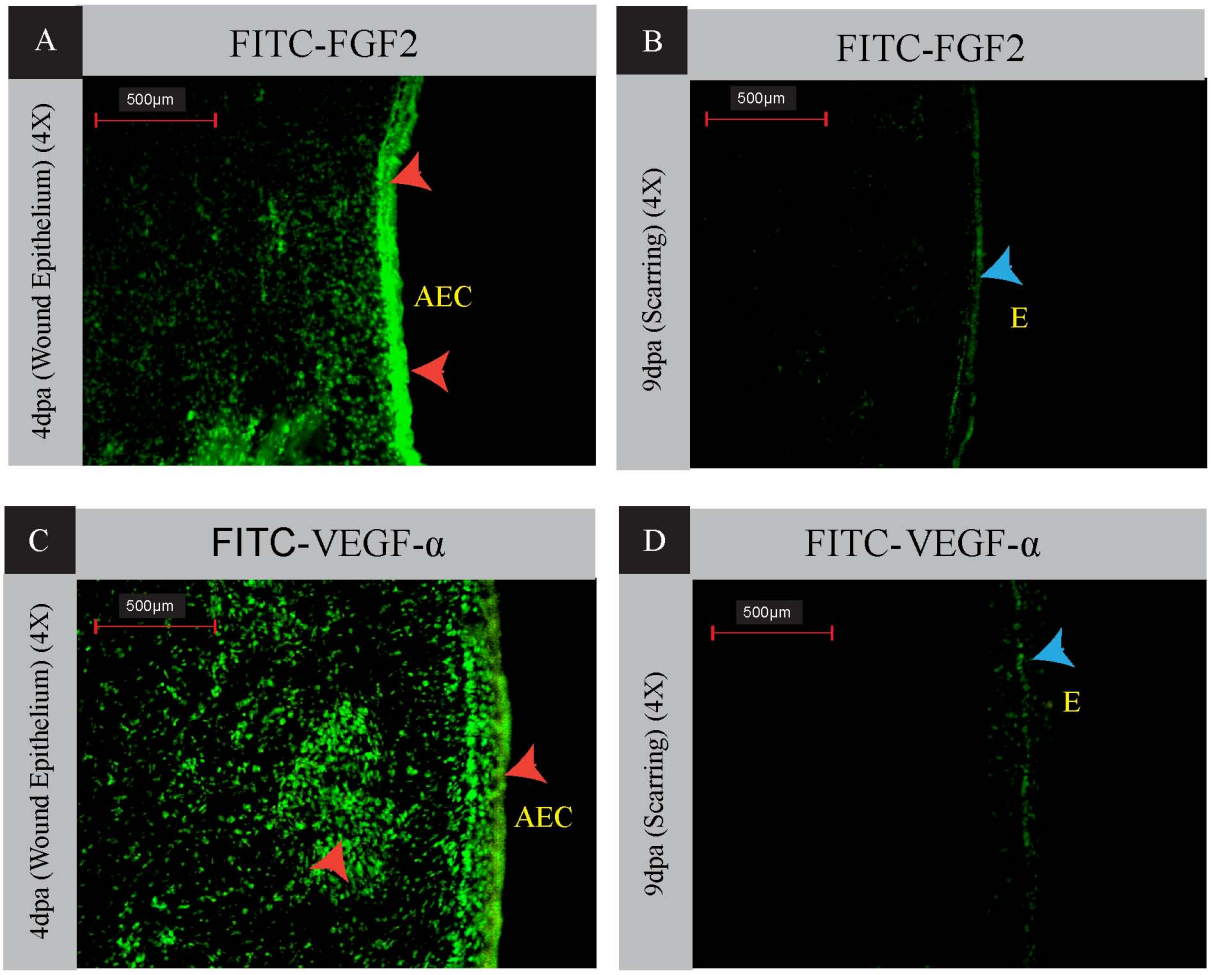

Figure 4.16: FGF2 and VEGF-α localization

A) indicates FGF2 localization in the AEC of tail at wound epithelium stage (orange arrowhead) and B) indicates faint localization signals of FGF2 in the limb healing stage (blue arrowhead). Figure C shows localization of VEGF-α in the proliferating epidermis and the underlying tissue (orange arrowhead) while it was present only in the epithelium of limb in a scattered manner (blue arrowhead) shown in figure D.

DISCUSSION

Lizards are amniote model of regeneration having the maximum evolutionary proximity to the mammals. Hence, there are similarities between the embryonic stages of reptiles and mammals (Lozito and Tuan, 2016). However, lizards are capable of regenerating the lost tail which unfortunately is not seen in mammals. Interestingly, lizards can restore only their tail but no other appendage via epimorphic regeneration (McClean and Vickaryous, 2011). Nonetheless, in order to facilitate regeneration of the tail, it needs to heal without the formation of a scar and hence, is called as scar-free wound healing. On the contrary, the amputated limb heals with a scar. Herein, an attempt was made to identify and compare the molecular differences in the mechanisms underlying scar-free and scarred wound healing in lizard.

In scar-free wound healing, the histological examination of the healing tail reveals a proliferating epidermis which at 2 dpa was 44.65 µm thick and increased its thickness to 91.93 µm by wound epithelium stage i.e. at 4 dpa. It is noticeable that the epidermis is continuously proliferating at the wound site as its thickness in the normal intact skin is only 12.52 µm. Similar results were observed by McLean and Vickaryous (2011) wherein the *Eublepharis* lizard shows a newly formed wound epithelium that continues to proliferate and thicken (up to 12 cell layers thick compared to 4-7 in the original epidermis), especially at the apical epithelial cap. In other regeneration models (e.g. urodeles, teleosts) the AEC has a well-documented role, as a source of morphogenetic information quite comparable to the apical ectodermal ridge of developing limb (Dinsmore, 1977; Poss et al., 2003). However, it is now accepted that under no circumstances formation of AEC happens in case of an amputated limb. Further, it has been documented that on amputation of a limb, the blood vessels rupture and the loss of blood is more as compared to that of the tail wherein the bleeding is kept at minimum due to contraction of precapillary sphincters (Delorme et al., 2012). Moreover, because of the prolonged bleeding in limb, a thick blood clot forms at the site of injury. Not surprisingly, on 3 dpa it was observed that the cut surface of the limb was covered only by a scab with no epithelial lining underneath as against the autotomy surface of tail wherein the epithelial covering was observed as early as on 1 dpa. However, on completion of wound closure at 9 dpa, a thick scar tissue of 200 µm covers the cut surface of limb and the overlying epidermis at this point is just 17 µm thickness, same as what used to be in a resting epithelial layer of limb, suggesting that AEC is not formed in limb and instead scarred stump is formed.

It has been well authenticated that the wound epithelium stratifies to form AEC through regulated cell division under the influence of various putative paracrine factors (Grose et al., 2002; Mescher, 2004). An upregulation in fgfs was observed, in all the time points studied, in the autotomized tail till the wound epithelium formation was accomplished at 4 dpa. *fgf1* and *fgf2* transcripts were found significantly higher in the healing tail and so was the FGF2 protein level, than in the resting one. A study by Alibardi (2012) showed positive immunolocalization for FGF2 in the epidermis of lizard tail which concurs with our findings wherein FGF2 was localized in the AEC and the underlying tissue, however limb showed positive staining only in the epithelium at the wound site suggesting a barrier formation between epithelium and underlying tissue which does not allow the cells to undergo proliferation. FGF2 and FGF1 are required for the epidermis to proliferate and form the AEC (Han et al., 2005; Alibardi and Lovicu, 2010; Yadav et al., 2012; Pillai et al., 2013). The same trend has been reported in chick limb development as well (Ornitz and Itoh, 2016), but in case of lizard limb healing, it was observed that these factors are either absent or their levels are too low to facilitate re-growth. FGF8 has a known role in the outgrowth of the limb of chick wherein it translocates from the epidermis to the underlying mesenchymal cells (Han et al., 2001). In lizard tail a steady increase of FGF8 was seen from 1 dpa to 4 dpa suggesting that its outgrowth must be very similar to that of the limb in a developing chick embryo. On the contrary, in the lizard limb, the absence of FGF8 may lead to stalling of outgrowth as well. In order to induce expression of FGF8, FGF10 is a prerequisite and there are ample evidences suggesting that FGF10 induces FGF8 in the ectoderm and Shh in mesoderm, proposing FGF10 to be an endogenous mesenchymal factor playing a pivotal role in initial budding and outgrowth of the vertebrate limb (Ohuchi et al., 1997; Xu et al., 1998; Ornitz and Itoh, 2016). The evidences mentioned above justifies the results in tail wound healing, wherein an increase in transcript level of *fgf10* along with *fgf8* was observed. The lack of *fgf8* and *fgf10* in lizard's limb would be playing a crucial role in the formation of the scarred stump at the amputated end. An increase in fgf8 and fgf10 leads to proliferation which was clearly seen in the western blot images of tail healing stages wherein a constant increase in PCNA was documented. Limb healing stages did show some increase in the protein levels of PCNA though not comparable to the tail, also their appearance was at a much later stage which might be due to collagen proliferation and deposition. To support this hypothesis, BrdU was incorporated in both tail and limb during healing, and the images clearly portray that BrdU gets accumulated in the AEC and the mesenchymal cells underlying it in tail while in limb, BrdU is seen only in the epithelium and the collagen deposited under it. Further evidences for proliferation and apoptosis were gathered from acridine orange and ethidium

bromide stained tissue sections. The tail tissue at wound epithelium stage (4 dpa) were predominated by proliferating cells. On the contrary, a corresponding stage in limb (9 dpa) revealed largely pro-apoptotic and apoptotic cells, indicating high apoptosis ensuing proper scar formation.

Apart from these FGFs mentioned above, another major factor required for sustaining the epidermis is FGF20 (Whitehead et al., 2005). FGF20 gets triggered by Wnt/β-catenin which in turn is regulated by ROS production. In *Xenopus* tadpole tail regeneration, higher levels of FGF20 were detected in the regenerating tissue when compared to the resting tissue (Love et al., 2013). In this study, tail which undergoes scar-free healing showed an increase in *fgf20* but the same was downregulated in limb again implying that the limb has an alternate path of healing which in due course leads to scarring.

Scarring is normally seen in mammalian injury, and limb healing in lizard also follows similar mechanism. The major growth factor that has a known role in scarring is the TGFβ (Klass et al., 2009; Kiritsi et al., 2017). One of the studies performed on human foetal skin revealed that if TGFβ1 and TGFβ2 cause scarring whereas in another study done on rat skin shows if expression of TGFβ3 in increased, the scarring reduces considerably (Soo et al., 2003; Larson et al., 2010). This leads to an inference, that TGFβ1 and TGFβ2 have a well-defined role in fibronectin deposition which was also observed during limb healing stages. In the light of the above discussion it could be presumed that for scar-less wound healing, deposition of fibronectin is avoided and hence *tgfβ3* was found to be elevated during tail wound healing stages. Not only does TGFβ have a role in fibrosis but it also plays a major role in inducing apoptosis (Perlman et al., 2001; Li et al., 2012). Lafon and coworkers (1996) found out that TGFβ1 induces apoptosis through c-fos and c-jun genes in human ovarian cancer cells. In the current study both TGFβ induced and p53 mediated apoptosis was studied for all the stages of healing in tail as well as limb. In tail, initially a 2-fold increase in *caspase 3* and *p53* was observed at 1 dpa and 2 dpa, however, these levels drop at 3 dpa and 4 dpa which also can be seen in the cleaved Caspase 3 immuno blot. In order to keep the tail growing, proliferation has to surpass apoptosis which was observed in this study wherein *p53, p21, bad, bax* and even the TGFβs were downregulated. Limb healing showed higher levels of *p53* and *p21* only at 9 dpa but a 200-fold surge was noted in *bad* expression at 6 dpa. This is because in scarred wound healing at granulation phase it is observed that the myofibroblasts disappear, leaving behind

the scar (Desmouliere, 1995). Apoptosis is a prerequisite for the entire mechanism and thus higher levels of bad at 6 dpa are justified.

Granulation phase is one of the important hallmarks of scarred wound healing (Sorg et al., 2017). During this stage, angiogenesis occurs and also fibroblast keep adding collagen, which eventually leads to scarring. At 6 dpa in limb, both *vegf-α* and *kdr* were seen to be high, again confirming that granulation might be starting at this point. In this phase, along with angiogenesis even deposition of collagen occurs which is induced by *tgfβ1* and *tgfβ2*. It is important to note that angiogenesis is required even for the successful realization of scar-free wound healing in tail, however the granulation phase here is highly truncated. In tail stump, the proliferating mesenchymal stem cells are maintained due to the virtue of high levels of *vegf-α* and *kdr*, which play a pivotal role in formation of blood vessels. VEGF-α was found to be localized in the AEC and more so in the underlying tissue from where actually the signals might be originating. Moreover, in case of tail, throughout all the time points, angiogenesis was observed, but it was noted in limb only at 6 dpa which was confirmed at protein level by western blot analysis. At 9 dpa though, as the scar matures, all the blood vessels retract, leaving behind only the fibrous tissue. To further validate this pathway, PI3K and Akt levels were checked for all the selected time point as these are the key molecules required for signalling. Both PI3K and Akt protein levels were constantly remained elevated in the tail starting 1 dpa while their levels were elevated in limb only at 6 dpa again confirming granulation to be occurring at this time point. Thus, with this it makes the events in which the healing is occurring quite clear for both scar-free and scarred wound healing.

Other studies carried out in lizard tail and limb healing are focused on specific stages of regeneration like wound healing and blastema in tail and scarring in limb. For instance, a study by Vitulo et al., (2017) in *Podarcis muralis* analyses the transcriptomic expression during tail and limb healing but specifically at the wound healing and blastema stages. The study did recognize wnt and fgfs for playing major roles in blastema recruitment which ultimately leads to regeneration of tail and failure of limb formation. Another study by Alibardi (2010) in *Podarcis sicula* reveals that cell proliferation is reduced in limb healing as compared to tail, an observation which coincides with the present study. Nevertheless, the results presented in the current work are based on a temporal expression pattern of some of the key molecules which are required to regulate various cellular events that facilitate the successful realization of the major milestones in the process of wound healing which has not yet been carried out in any of

the lizard models. Through this study it can be construed that the central events like proliferation, apoptosis and angiogenesis do occur in both scar-free as well as in scarred wound healing, but the duration for which they last and the point at which these are patterned, differs and this difference causes the tail to follow scar free healing, while the limb undergoes the scarred wound healing process.

CONCLUSION

Lizards are unique in having both - regeneration competent (tail) as well as non-regenerating appendages (limbs) in adults. They therefore, present an appropriate model for comparing processes underlying regenerative repair and non-regenerative healing after amputation. In the current study, we used northern house gecko *Hemidactylus flaviviridis* to compare major cellular and molecular events following amputation of the limb and of the tail. Although the early response to injury in both cases comprises apoptosis, proliferation and angiogenesis, the temporal distribution of these processes in each remained obscure. In this regard, observations were made on the anatomy and gene expression levels of key regulators of these processes during the healing phase of the tail and limb separately. It was revealed that cell proliferation markers like FGFs were upregulated early in the healing tail, coinciding with the growing epithelium. The amputated limb, in contrast, showed weak expression of proliferation markers, limited only to fibroblasts in the later stage of healing. Additionally, apoptotic activity in the tail was limited to the very early phase of healing, as opposed to that in the limb, wherein high expression of cleaved Caspase 3 was observed throughout the healing process. Early rise in VEGF-α expression reflected an early onset of angiogenesis in the tail, while it was seen to occur at a later stage in case of the limb. Moreover, the expression pattern of TGF-β members points towards a pro-fibrotic response being induced very early in the amputated limb. Collectively, these results explain why regenerating appendages are able to heal without scars and if we are to induce scar-free healing in non-regenerating limbs, what interventions can be envisaged. This is crucial to the field of regenerative medicine since it is the initial stages of repair following amputation, which decide whether the appendage will be restored or only covered with a scab.

SUMMARY

Lizards achieve the wound epithelium stage at 4 dpa whereas the limb requires 9 dpa for full wound closure. Various processes and signalling molecules play an important role in deciding the course of healing. In this study, it was observed that proliferation of epidermal cells and the mesenchymal cells is triggered as soon as the there is an injury to the tail, however the limb shows proliferation only of the fibroblast cells at a later stage of healing. Various fgf genes were found upregulated in order to form the proliferating epidermis which eventually forms AEC at 4 dpa in tail. The proliferation of epidermal cells follows the activation of PI3K-Akt signalling pathway as their levels were found to be elevated along with fgfs. Instead of proliferation at an early stage, limb showed apoptosis to be persistent for a longer duration wherein the expression of *bad* and *caspase 3* were seen at an early stage at 3 dpa and *caspase* remained high till later stage along with *p53* and *p21* which is triggered by the p38-MAPK pathway as evident from the result. Apoptosis was apparent at 1 dpa in tail but it was subsequently found to be downregulated. Apart from fgfs, tgf-β members are also a pre-requisite in wound healing and the results suggest that *tgf-β1* and *tgf-β2* are involved in the scarring and apoptosis as their levels were significantly high in the stages of limb wound healing. In contrast to this, *tgf-β3* promotes scar-free wound healing which are in agreement with the results obtained from the tail wound healing stages. Apart from these two processes, angiogenesis which is the primary requirement to sustain the proliferation was also recorded in both the wound healing. In tail, angiogenesis occurred at an early stage to provide a proliferating environment for the epidermis while in limb at a very late stage this process was observed. Hence VEGF-α levels were elevated throughout the process of wound healing in tail, these levels shot up only at 6 dpa, which is the granulation phase in the limb which eventually leads to scarring. Thus, all these three processes depicted in Figure 4.17, play a major role in scar-free and scarred wound healing. Even though they all occur in both the wound healing their occurrence and duration are quite different which may be the reason which allows the tail to heal in scar-free manner and regain it completely whereas the limb undergoes scarred wound healing which ultimately forms a stump with no functionality.

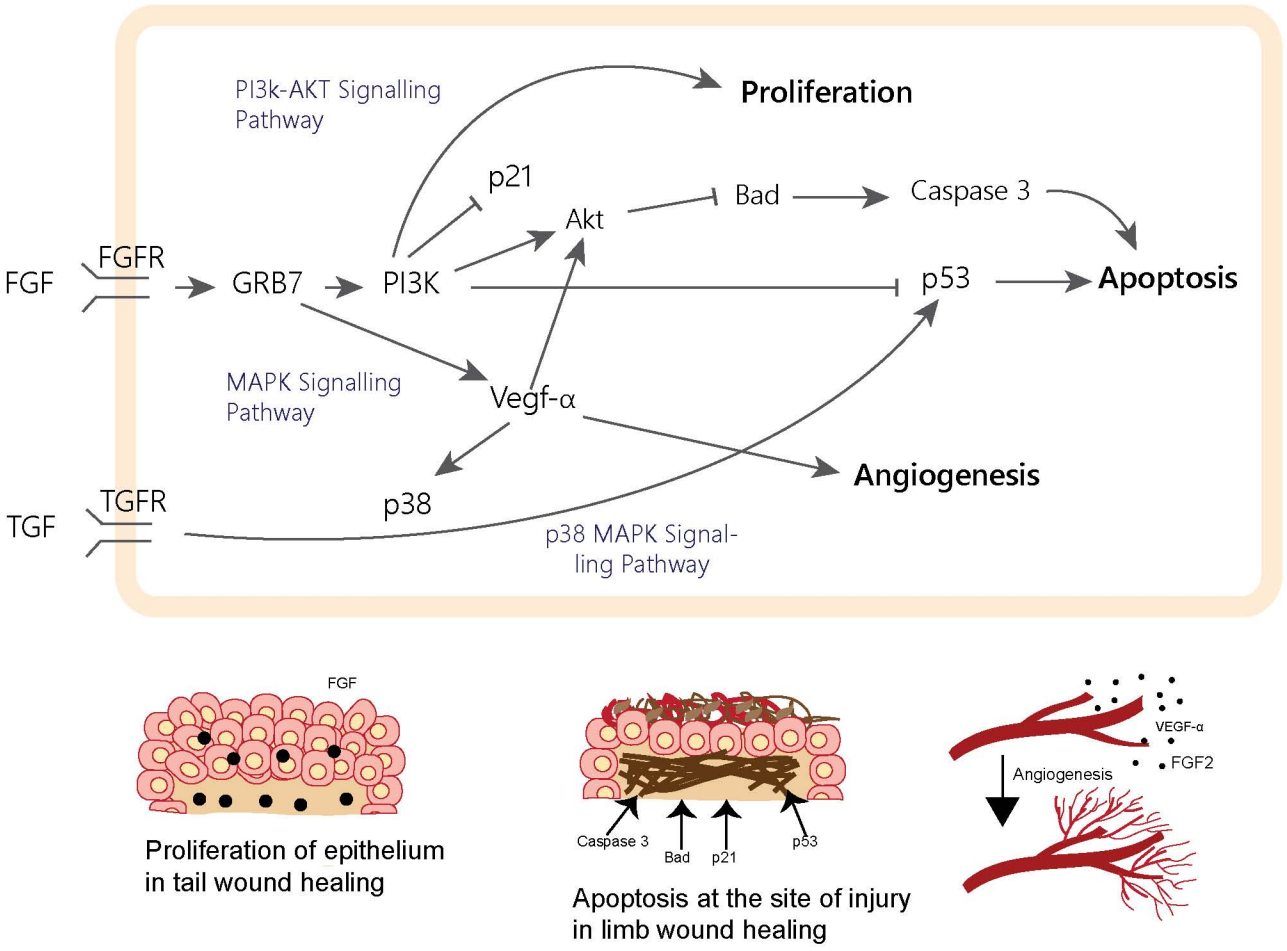

Figure 4.17: Cellular processes and the molecules involved in scar-free and scarred wound healing in *Hemidactylus flaviviridis*.